Calibration of Linear Contact Stiffnesses in Discrete Element Models Using a Hybrid Analytical-Computational Framework

Tongming Qu[a], Y.T. Feng[a*], T. Zhao[a], Min Wang[b]

[a]Zienkiewicz Centre for Computational Engineering, College of Engineering, Swansea University, Swansea, Wales SA1 8EP, UK

[b]T-3 Fluid Dynamics and Solid Mechanics Group, Theoretical Division, Los Alamos National Laboratory, Los Alamos, New Mexico, 87545, USA

*Corresponding author; e-mail: y.feng@swansea.ac.uk

Abstract

Efficient selections of particle-scale contact parameters in discrete element modelling remain an open question. The aim of this study is to provide a hybrid calibration framework to estimate linear contact stiffnesses (normal and tangential) for both two-dimensional and three-dimensional simulations. Analytical formulas linking macroscopic parameters (Young's modulus, Poisson's ratio) to mesoscopic particle parameters for granular systems are derived based on statistically isotropic packings under small-strain isotropic stress conditions. By taking the derived analytical solutions as initial approximations, the gradient descent algorithm automatically obtains a reliable numerical estimation. The proposed framework is validated with several numerical cases including randomly distributed monodisperse and polydisperse packings. The results show that this hybrid method practically reduces the time for artificial trials and errors to obtain reasonable stiffness parameters. The proposed framework can be extended to other parameter calibration problems in DEM.

Keywords: Discrete element method; Homogenisation methods; Constitutive law; Contact force chains; Calibration method; Gradient descent.

1 Introduction

The discrete element method (DEM) is widely employed to analyse the mechanical behaviour of granular materials in many engineering fields. Reliable DEM simulations can only be performed if particle parameters contained in DEM contact models are reasonably selected. However, the appropriate choice of these model parameters at the particle level, i.e. the model parameter calibration, still remains as one of main obstacles for a wider application of DEM to engineering problems [1, 2].

There are two approaches that are generally used to determine particle-level model parameters in DEM, namely the *direct measuring approach* and the *bulk calibration approach* [3]. The direct measuring approach measures the properties at the particle or contact level. Some properties for certain particles, such as glass or steel beads, are easy to be measured but may be difficult for most of particles, such as sand.

DEM models typically simplify the complexity of a real physical system, particularly in terms of particle geometry, contact interaction, and the number of particles involved. Thus even if particle-scale properties can be measured accurately, it does not mean that the system represented by DEM can exhibit the same level of accuracy as the real system at the macroscopic level [4]. Consequently, the aim of parameter calibration is to acknowledge the simplifications made in DEM models and to adjust the particle-scale parameters to capture the salient mechanical behaviour observed in physical tests [5, 6]. Based on this idea, the so-called bulk calibration approach is developed as a mainstream method to calibrate parameters in DEM.

The calibration of DEM parameters with bulk material behaviour is a process of determining the causal factors (mesoscopic parameters) from a set of observations or measures (macroscopic results) and is thus an *inverse problem*. The corresponding *forward problem* is estimating or predicting the macroscopic stress-strain behaviour

(also called constitutive relations) of a particle assembly based on particle-scale parameters. This forward problem is of great interest to physics, soil mechanics, and material science and has received a large number of considerations. As a foundation to address the calibration of DEM parameters, constitutive laws of granular materials and the corresponding homogenisation methods are revisited in Section 2.

The bulk calibration approach requires physical experiments as a match target of DEM models. Except for bi-axial and tri-axial tests that are commonly used for the calibration of confined granular materials, many physical experiments have been introduced to calibrate the mesoscopic parameters, such as cylindrical mixer apparatus [7], static packing pressure test [8], and lifting cylinder tests [9]. Although simpler experiments have been introduced, large amount of time for trials and errors is still required [3, 10-13]. Some researchers use the sensitivity tests of different parameters on the bulk properties to accelerate the selection of appropriate parameters [3], but the calibration process is still very time-consuming and inefficient.

Another recent development of the bulk calibration approach is the use of statistical algorithms to determine mesoscopic parameters in DEM, such as response surface methodology [14], artificial neural networks [15, 16], Latin hypercube sampling and Kriging [17], random forest [18], genetic algorithm [19, 20], sequential quasi-Monte Carlo [21] and Bayesian approach [22]. Although these statistical algorithms allow researchers to quantify a wide range of phenomena and seem to serve as a panacea for many complex problems, they simply provide an empirical approximation and cannot replace the study on underlying physical laws.

As the first part of a series of work to address some of parameter calibration problems in DEM, the aim of this paper is to provide a hybrid analytical-computational framework that can robustly estimate the particle-scale stiffness

parameters in the linear contact model for *disc*/*spherical* particle assemblies. On the basis of a brief review on commonly used homogenisation methods, a set of continuum-based theoretical formulae between particle-scale stiffnesses and macro material properties are explicitly formulated based on *kinematic hypothesis*. These analytical formulae are checked with the numerical solutions for wide ranges of porosities and stiffness ratios. By using the derived analytical solutions as the initial values, a gradient descent technique is then proposed to predict more reliable particle-scale stiffness values for general granular systems.

The paper is organised as follows: Section 2 derives a general constitutive relation for a granular assembly and then further develops it to a simplified analytical version suitable for explicitly formulating particle stiffnesses. Section 3 designs two groups of biaxial/triaxial numerical test cases to illustrate main differences between the derived formulas and numerical results for both monodisperse particle packings and polydisperse particle packings. Section 4 proposes a hybrid analytical-computational framework in which the formulas derived in Section 3 is used to obtain the initial estimation of the two contact stiffnesses and then a gradient descent based computational procedure is employed to further refine the prediction of the parameters.

2 Constitutive laws for granular assemblies

2.1 A brief review of the homogenisation method

The homogenisation method has played an important role in obtaining constitutive laws of granular materials. Acting as a bridge connecting the macro-scopic stress-strain responses and particle-scale parameters, various homogenisation methods have been developed to derive constitutive relations of granular materials. Some commonly

used homogenisation methods are briefly reviewed below.

2.1.1 Voigt's hypothesis

Voigt's hypothesis (also called the kinematic assumption) assumes that the strain in the material is uniform. This hypothesis enables determining the local displacement field from the global strain [23]. Such a displacement field in accordance with the uniform strain is also called the "mean displacement field". Voigt's hypothesis has been used to describe the displacement field of granular packings [24-26]. However, the hypothesis restricts the possible movement of particles (kinematic constraint) and yields an upper-bound solution [27]. Even though some improvement has been made by considering more elaborate factors, such as the particle rotation effect, the derived solution still significantly overpredicts the actual values [28]. Based on the minimum potential energy principle, the Young's modulus derived from Voigt's hypothesis is proved to be an upper bound solution [29].

2.1.2 Reuss's hypothesis

Apart from Voigt's hypothesis based on the uniform strain, another well-known hypothesis comes from the idea that all stress components in granular material are uniform and is called *Reuss's hypothesis* or the *static assumption* [30]. Reuss's hypothesis generally deduces the local contact forces from the global uniform stress [23]. Based on the minimum complementary energy principle, the modulus derived from Reuss's hypothesis is proved to be a lower bound solution [29]. Some constitutive relationships of granular materials based on Reuss's hypothesis can be found in [31, 32].

2.1.3 Best fit hypothesis and Piece-wide fit hypothesis

The *best fit hypothesis* is developed based on the observation that the actual displacement field in granular materials does not coincide with but fluctuate about the mean displacement field. By minimising the difference between the actual contact displacement and the mean field displacement, the relation between the macroscopic strain and the particle-scale displacement field can be established [27]. The application of the best fit hypothesis on deriving constitutive relationships of granular packings can be found in [27, 33]. The best-fit strain approaches are reportedly inconsistent with local force equilibrium in randomly disordered granular packings and thus give rise to an uncontrolled approximation of the strain field [34].

Although the averaged strain of a particle assembly can be obtained from the best fit of the displacement field, the actual strain is non-uniform in the amorphous granular packing. To capture the feature of non-uniform strain at the particle scale, a scheme of *piece-wise fit* to the displacement field is introduced in [27]. To this end, a concept of the "local region" is defined to represent a particle and its vicinity. By fitting the displacement conditions at each "local region", a local strain can be introduced. Then the overall strain for the entire granular packing can be obtained by averaging all the local strains. Basically, the piece-wide fit hypothesis considers the effect of the particle-scale fabric variation due to the structural heterogeneity of a granular packing and can be regarded as a conceptual improvement of the best fit hypothesis. However, the piece-wide fit hypothesis is seldom reported by follow-up studies, probably due to the extreme complexity of its derived formulation.

2.1.4 Affine and non-affine fields

This method originates from the understanding that particle displacements in

amorphous materials do not conform to the imposed affine strain. This observation leads to the idea of decomposing particle displacements into affine parts and non-affine parts. By subtracting the expected homogeneous deformation, the non-affine velocity or displacements fields can be obtained in simulations of granular materials [35, 36].

These non-affine displacements or "noise" are typical of the same order of magnitude as the relative affine displacement of neighbouring particles, and thus cannot be regarded as a small correction. Ignoring the "noise" displacements (as in both Voigt's and Reuss's hypothesises) or treating them as a limited perturbation (as in the best fit hypothesis and the piece-wide fit hypothesis) yields inaccurate predictions for macroscopic properties [37, 38]. A constitutive relation of granular materials based on the understanding of non-affine displacements is derived in [34, 39]. However, as the derived Young's modulus highly depends on the artificial choice of the coarse-graining function, this method has not been widely used.

2.1.5 Other methods

Various homogenisation theories can be found in the existing literature. The *self-consistent hypothesis* is developed by Hershey [40] to find the effective Young's moduli for aggregates of crystals. It divides the macro-scopic quantity (such as strain or stress) in aggregates into the local uniform quantity in the component and the far-field uniform quantity component of the aggregate. Depending on the selected macroscopic quantity, the method can degenerate into Voigt's hypothesis or Reuss's hypothesis if the local strain or stress equals to the far-field counterpart [41].

The method based on Voronoi-Delaunay tessellations is also used to describe the internal structure of granular materials [42, 43]. To facilitate stress-strain analysis of

granular materials, the tessellation of a two-cell system including both solid cell space and void cell space is further studied [44]. The particle-scale Voronoi-Delaunay tessellations can reflect the spatial arrangement of a granular assembly and can be partly regarded as an improvement of the before-mentioned piece-wide fit hypothesis. Furthermore, Voigt's or Reuss's hypothesis can be applied to each Voronoi cell to obtain the constitutive relation [23]. Although this Voronoi-Delaunay tessellation based method is conceptually attractive, its mathematical expressions incorporating stress-strain relations are highly sophisticated. Particularly the macroscopic material parameters (Young's modulus and Poisson's ratio) of granular materials are hard to be explicitly expressed.

2.1.6 Brief summary

Constitutive relations of granular materials have been developed in science and engineering fields. Although various hypothesises are involved and sophisticated formulations have been derived, the accurate prediction of constitutive relations of granular materials remains to be an outstanding issue. In the absence of accurate constitutive relations, the relations between macro material parameters, such as Young's modulus and Poisson's ratio, and mesoscopic parameters, such as contact stiffnesses, cannot be established. As a result, the determination of reasonable particle-scale stiffness values used for DEM analysis is still difficult.

The reason for failure to accurately predict constitutive relationships of granular materials may be attributed to the fact that most homogenisation methods are derived from the continuum-based theory. The existing literature has shown that the continuum elasticity is valid only under certain conditions for granular materials [45, 46]. Granular systems, whether spatially disordered or ordered particle packings, are

observed to transfer forces in a chain-like way when subjected to external loads [47, 48]. It is the fact that force propagation along force chains does not preclude elasticity of granular matter, but it is understandable that the continuum theory cannot be expected to describe the mesoscopic inter-particle forces perfectly, even in the small-strain elastic stage [45]. Although numerous attempts have been made toward the characterisation of force networks in granular matters, the current knowledge about force chains is still inadequate to connect the micro elasticity to the macro elasticity (continuum-based mechanics).

In the following subsections, a set of kinematic solutions is derived based on the strain energy formulation in Section 2.2, and a set of simplified kinematic solutions is further obtained under the condition of isotropic assumption. The derived simplified kinematic solution will be evaluated with numerical solutions in Section 3.

2.2 General Relation between mesoscale stiffnesses and macroscale elastic constants

Basically, two kinds of elastic contact models without bond are commonly used in DEM. One is the linear contact model and the other is the non-linear Hertz contact model [5]. In this study, based on the assumption that the deformation of the granular assembly is statistically uniform in the space (Voigt's hypothesis), the particle-scale parameters in the linear contact model are derived. The reasons for choosing Voigt's hypothesis are not just because of its concise formulation but also the reported reliability in terms of capturing the stress-strain behaviour of granular materials.

The fundamental idea of matching particle-scale parameters and macro material parameters is the equivalence of strain energy between a granular system and the corresponding continuum:

$$U_{discrete} = U_{continuum} \tag{1}$$

The strain energy is equal to the work done by the contact forces which act from the un-deformed state until the state of the current deformation [49]. It should be noted that only displacements in both normal and tangential contact directions are responsible for changes in strain energy of the equivalent continuum because the topology of a disc/spherical particle assembly is independent of the rotations of particles [50], and no rolling stiffness and damping are considered. The total strain energy stored in the entire system is given by:

$$U = \sum_{k=1}^{N_c} \left(\int_0^{\Delta u_n^k} F_N d\delta_n + \int_0^{\Delta u_s^k} F_s d\delta_s \right) \tag{2}$$

where Δu_n^k and Δu_s^k denote the normal and tangential relative displacements of contact k, respectively; F_n and F_s are contact forces in the normal and shear directions, respectively; $d\delta_n$ and $d\delta_s$ are infinitesimal deformations in the normal and shear directions, respectively; and N_c is the total number of contacts excluding the contacts with zero force in the entire granular system because only the contacts carrying forces contribute to the mechanical balance [51].

For the linear contact model in DEM, the contact forces can be expressed with contact relative displacements as follows:

$$F_N = K_n \Delta u_n, \; F_s = K_s \Delta u_s \tag{3}$$

where K_n and K_s are the normal and tangential stiffnesses of the contact; Δu_n and Δu_s are the normal and tangential relative displacements of the contact, respectively. It should be noted that Eq. (3) is only valid within the Coulomb limit. i.e., the tangential force is equal or less than the maximum friction force.

The strain energy stored in contact k with a linear contact relation is given by:

$$U^k = \frac{1}{2}\left(K_n \Delta u_n^k \Delta u_n^k + K_s \Delta u_s^k \Delta u_s^k\right) \tag{4}$$

By equating the particle displacements to the displacements of the corresponding points in the continuum, the relationship between the relative displacement of particles Δu_i^k and the equivalent local strain ε_{ij}^k in the continuum is determined as:

$$\Delta u_i^k = \varepsilon_{ij}^k (x_j^{(B)} - x_j^{(A)}) = \varepsilon_{ij}^k L^k \xi_j{}^k \tag{5}$$

where $x_j^{(A)}$ and $x_j^{(B)}$ are the coordinates of particles A and B in the x_j direction; L^k is the distance of contact k (between the centres of particles A and B here); and $\xi_j{}^k$ is the j-component of the direction vector of contact k. The normal relative displacement Δu_n^k can be expressed as

$$\Delta u_n^k = \Delta u_i^k \xi_i^k = \varepsilon_{ij}^k (x_j^{(B)} - x_j^{(A)}) \xi_i^k = \varepsilon_{ij}^k L^k \xi_i^k \xi_j{}^k \tag{6}$$

The tangential relative displacement Δu_s^k can be written as

$$\Delta u_s^k = \Delta u_i^k - \Delta u_n^k = \varepsilon_{mn}^k L^k \xi_n{}^k - \varepsilon_{ij}^k L^k \xi_i^k \xi_j{}^k \xi_m{}^k \tag{7}$$

Substituting Eqs. (6) and (7) into (4), the energy stored in the granular system with the linear contact relation can be rewritten as:

$$U = \sum_k^{Nc} U^k = \frac{1}{2}\sum_{k=1}^{N_c}\left[K_n \varepsilon_{ij}^k L^k \xi_i^k \xi_j^k \varepsilon_{mn}^k L^k \xi_m^k \xi_n^k + K_s (\varepsilon_{kl}^k L^k \xi_l{}^k - \varepsilon_{ij}^k L^k \xi_i^k \xi_j^k \xi_k^k)(\varepsilon_{km}^k L^k \xi_m^k - \varepsilon_{mn}^k L^k \xi_m^k \xi_n^k \xi_k^k)\right] \tag{8}$$

Then the strain energy density for the whole system is given by:

$$u = \begin{cases} \dfrac{U}{S} & \text{(2D model)} \\ \dfrac{U}{V} & \text{(3D model)} \end{cases} \tag{9}$$

where S is the total domain area of the particle assembly in the 2D case, while V is the total volume in the 3D case. In what follows, we derive the formulas for 3D cases, while the properties in 2D cases can be readily obtained by ignoring the third index

and replacing V by S.

According to the theory of elasticity, the stress tensor of a continuum can be obtained by differentiating the strain energy density with respect to the corresponding strain tensor as follows:

$$\sigma_{ij} = \frac{\partial u}{\partial \varepsilon_{ij}} \tag{10}$$

We assume that the macro material properties of a granular assembly are statistically uniform in the space, so a local strain in any position for the corresponding continuum equals to the overall strain:

$$\varepsilon_{ij} = \varepsilon_{ij}^{k} \tag{11}$$

Therefore Eq. (10) for the corresponding continuum can be expressed as:

$$\sigma_{ij} = \frac{1}{V}\sum_{k=1}^{Nc}\frac{\partial U^{k}}{\partial \varepsilon_{ij}^{k}} = \frac{1}{V}\sum_{k}^{N_c}\left[K_n \varepsilon_{ij}^{k} L^{k} \xi_i^{k} \xi_j^{k} \varepsilon_{mn}^{k} L^{k} \xi_m^{k} \xi_n^{k} + K_s(\varepsilon_{ik}^{k} L^{k} \xi_k^{k} \xi_j^{k} - \varepsilon_{mn}^{k} \xi_i^{k} \xi_j^{k} \xi_m^{k} \xi_n^{k})\right] \tag{12}$$

The elastic stiffness tensor can be obtained by differentiating the stress component with respect to the corresponding strain component as:

$$\begin{aligned} C_{ijmn} = \frac{\partial \sigma_{ij}}{\partial \varepsilon_{mn}} = \frac{\partial \sigma_{ij}}{\partial \varepsilon_{mn}^{k}} &= \frac{1}{V}\sum_{k=1}^{N_c}\left[K_n \left(L^{k}\right)^{2} \xi_i^{k} \xi_j^{k} \xi_m^{k} \xi_n^{k} + K_s \left(L^{k}\right)^{2} (\delta_{in} \xi_j^{k} \xi_m^{k} - \xi_i^{k} \xi_j^{k} \xi_m^{k} \xi_n^{k})\right] \\ &= \frac{(K_n - K_s)}{V}\sum_{k=1}^{N_c}\left(L^{k}\right)^{2} \xi_i^{k} \xi_j^{k} \xi_m^{k} \xi_n^{k} + \frac{K_s}{V}\sum_{k=1}^{N_c}\left(L^{k}\right)^{2} \delta_{in} \xi_j^{k} \xi_m^{k} \end{aligned} \tag{13}$$

where δ_{in} is Kronecker's delta function. The physical meaning of C_{ijmn} is the stiffness for tension or compression in one principal direction when strains in the other directions (perpendicular to the principal direction) are constrained to be zero. Both terms $\sum_{k=1}^{N_c}\left(L^{k}\right)^{2} \xi_i^{k} \xi_j^{k} \xi_m^{k} \xi_n^{k}$ and $\sum_{k=1}^{N_c}\left(L^{k}\right)^{2} \delta_{in} \xi_j^{k} \xi_m^{k}$ in Eq.(13) are purely determined by the packing structure of a granular assembly and can be determined once the fabric components of particles are known (it is easy to do in a numerical model).

Although granular assemblies are inherently amorphous and heterogeneous in general, the mechanical behaviour of a granular assembly can still be regarded as an elastic body in the case of small deformation. The usual constitutive formulations for general elastic media, either iso- or aniso-tropic, are well-established in solid mechanics. The relation between the equivalent elastic parameters and the particle-scale parameters can be established based on the established formulation. For example, the elastic stiffness tensor C_{ijmn} for isotropic elastic solid is given as:

$$C_{ijmn} = \frac{E}{2(1+\nu)}(\delta_{in}\delta_{jm} + \delta_{im}\delta_{jn}) + \frac{E\nu}{(1+\nu)(1-2\nu)}\delta_{ij}\delta_{mn} \tag{14}$$

where E and ν are Young's modulus and Poisson's ratio, respectively.

By comparing Eq.(13) with Eq.(14), the equivalent Young's modulus and Poisson's ratio in an isotropic granular assembly can be obtained. Eq.(13) unveils the fundamental relation between the particle-scale stiffness, fabric configuration and equivalent macroscale deformation parameters. For a specific packing assembly, the equivalent elastic parameters can be determined by combining the packing structure and the known particle stiffnesses. On the other hand, we can understand how the macro deformation of granular material is related to the fabric configuration without considering particle breakage and deterioration. For simplicity, a more simplified constitutive law will be derived in the next section.

2.3 A simplified constitutive law for the granular assembly with an isotropic structure

Eq.(13) is a generalised description and can be applied to any particle packing. Under the condition that all particles are of equal size and have the same material properties, Eq. (13) can be simplified as:

$$C_{ijmn} = \frac{4r^2(K_n - K_s)}{V}\sum_{k=1}^{N_c}\xi_i^k\xi_j^k\xi_m^k\xi_n^k + \frac{4r^2K_s}{V}\sum_{k=1}^{N_c}\delta_{in}\xi_j^k\xi_m^k \tag{15}$$

where r is the radius of particles. Similar results have already been found in [27, 29, 52, 53].

For a granular assembly with a large number of particles and contacts, the orientations of contact normals can be assumed to obey a statistically even distribution. Eq. (15) can thus be expressed in a continuum form. Let the distribution density function of particle contacts be $\rho(\theta)$ or $\rho(\gamma,\beta)$, where θ is the angle in the polar coordinate system (2D, Fig. 1a), and γ and β are the angles in the spherical coordinate system (3D, Fig. 1b). The density function of contacts represents the number of contacts that direct to a certain angle in space and therefore satisfies the condition:

$$\begin{cases} \int_0^{2\pi} \rho(\theta) d\theta = 1 & \text{(2D)} \\ \int_0^{2\pi}\int_0^{\pi} \rho(\gamma,\beta)\sin\gamma d\gamma d\beta = 1 & \text{(3D)} \end{cases} \tag{16}$$

The number of contacts in a local area $d\Omega$ is given as $N_c\rho(\theta)d\Omega$ or $N_c\rho(\gamma,\beta)d\Omega$, where N_c is the total number of contacts in the volume V.

Under the condition that the particle assembly is statistically isotropic or quasi-isotropic, the distribution density function has the form:

$$\begin{cases} \rho(\theta) = \dfrac{1}{2\pi} & \text{(2D)} \\ \rho(\gamma,\beta) = \dfrac{1}{4\pi} & \text{(3D)} \end{cases} \tag{17}$$

Replacing the summation in Eq. (15) by integration leads to:

$$C_{ijmn} = \begin{cases} \dfrac{4r^2(K_n-K_s)}{V}\dfrac{N_c}{2\pi}\int_\Omega \xi_i\xi_j\xi_m\xi_n d\Omega + \dfrac{4r^2K_s}{V}\dfrac{N_c}{2\pi}\int_\Omega \delta_{in}\xi_j\xi_m d\Omega & \text{(2D)} \\ \dfrac{4r^2(K_n-K_s)}{V}\dfrac{N_c}{4\pi}\int_\Omega \xi_i\xi_j\xi_m\xi_n d\Omega + \dfrac{4r^2K_s}{V}\dfrac{N_c}{4\pi}\int_\Omega \delta_{in}\xi_j\xi_m d\Omega & \text{(3D)} \end{cases} \tag{18}$$

Here $\int_\Omega (\bullet) d\Omega = \int_0^{2\pi} (\bullet) d\theta$ for the 2D case and $\int_\Omega (\bullet) d\Omega = \int_0^{2\pi}\int_0^{\pi} (\bullet)\sin\gamma d\gamma d\beta$ for the

3D case. So Eq. (18) can be reduced to:

$$C_{ijmn}=\begin{cases}\dfrac{2N_c r^2(K_n-K_s)}{V\pi}\int_0^{2\pi}\xi_i\xi_j\xi_m\xi_n d\theta+\dfrac{2N_c r^2K_s}{V\pi}\int_0^{2\pi}\delta_{in}\xi_j\xi_m d\theta & \text{(2D)}\\ \dfrac{N_c r^2(K_n-K_s)}{V\pi}\int_0^{2\pi}\int_0^{\pi}\xi_i\xi_j\xi_m\xi_n\sin\gamma d\gamma d\beta+\dfrac{N_c r^2K_s}{V\pi}\int_0^{2\pi}\int_0^{\pi}\delta_{in}\xi_j\xi_m\sin\gamma d\gamma d\beta & \text{(3D)}\end{cases} \tag{19}$$

In the polar or spherical coordinate system, a contact normal can be represented as:

$$\boldsymbol{\xi}=\begin{cases}(\cos\theta,\sin\theta) & \text{(2D)}\\ (\sin\gamma\cos\beta,\sin\gamma\sin\beta,\cos\gamma) & \text{(3D)}\end{cases} \tag{20}$$

By substituting Eq. (20) into Eq. (19) and evaluating the integrals, the elastic stiffness tensor can be explicitly expressed as:

$$C_{ijmn}=\begin{cases}\dfrac{N_c r^2(5K_n+3K_s)}{8V}(\delta_{in}\delta_{jm}+\delta_{im}\delta_{jn})+\dfrac{N_c r^2(K_n-K_s)}{4V}\delta_{ij}\delta_{mn} & \text{(2D)}\\ \dfrac{2N_c r^2(2K_n+3K_s)}{15V}(\delta_{in}\delta_{jm}+\delta_{im}\delta_{jn})+\dfrac{4N_c r^2(K_n-K_s)}{15V}\delta_{ij}\delta_{mn} & \text{(3D)}\end{cases} \tag{21}$$

By comparing Eq. (21) with the usual expression of stiffness tensor (see Eq.(14)) in solid mechanics, we have

$$E=\begin{cases}\dfrac{2N_c r^2K_n}{V}\left(\dfrac{5K_n+3K_s}{7K_n+K_s}\right) & \text{(2D)}\\ \dfrac{4N_c r^2K_n}{3V}\left(\dfrac{2K_n+3K_s}{4K_n+K_s}\right) & \text{(3D)}\end{cases} \tag{22}$$

$$\nu=\begin{cases}\dfrac{K_n-K_s}{7K_n+K_s} & \text{(2D)}\\ \dfrac{K_n-K_s}{4K_n+K_s} & \text{(3D)}\end{cases} \tag{23}$$

As the above closed-form solutions are derived based on the assumption that all of the strain components throughout the model are uniform (i.e. the Voigt hypothesis [30]), the corresponding solution is called a kinematic solution [54]. For convenience, Eq. (13) is termed the generalised kinematic solution, and Eq. (21) and its derived Eqs. (22) and (23) are called the simplified kinematic solutions. The error due to introducing such a statistically isotropic simplification will be investigated in the next section.

3 Comparison between numerical tests and derived formula

3.1 Test schemes

To fully determine the equivalent elastic properties of a 2D granular assembly, including Young's modulus E and Poisson's ratio v, two loading cases are employed in biaxial/triaxial tests. One is to keep the lateral confining stress constant (shown in Fig. 2a) while the other is to keep the lateral boundary fixed (see Fig. 2b), during axial compression testing.

In the case of a constant confining stress, the equivalent elastic modulus of granular materials can be numerically given by:

$$E = (\frac{\Delta\sigma}{\Delta\varepsilon})_c \tag{24}$$

where the subscript index c represents a constant confining stress condition.

The specimen is loaded along the vertical direction until the axial strain is up to a relatively small value (5×10^{-4} is adopted in our model). Here a loading-unloading case can be used to check whether or not the granular specimen is in a state of elastic deformation during loading/unloading.

According to the second case which keeps the lateral boundary fixed, the elastic constants E and v of the specimen can be determined by the slope of the axial deviatoric stress versus the axial strain as:

$$\frac{E(1-v)}{(1+v)(1-2v)} = (\frac{\Delta\sigma}{\Delta\varepsilon})_f \tag{25}$$

where the subscript index f represents a fixed boundary condition.

The combination of the above two tests can determine the Poisson's ratio of a specimen under small strain. We define a constant n as the ratio of the slope of stress-strain in the fixed boundary condition to the slope of stress-strain in the constant

confining stress condition:

$$n = \frac{(\frac{\Delta\sigma}{\Delta\varepsilon})_f}{(\frac{\Delta\sigma}{\Delta\varepsilon})_c} \tag{26}$$

Then the Poisson's ratio can be determined as:

$$\nu = \frac{(1-n)+\sqrt{9n^2-10n+1}}{4n} \tag{27}$$

The above test schemes will be adopted for the following both monodisperse and polydisperse packings to determine the equivalent Young's modulus and Poisson's ratio.

3.2 Monodisperse particle packing

As shown in Fig. 3, a granular assembly with monodisperse (equal-sized) particles enclosed in a square/cubic box is generated with Particle Flow Code (PFC) software [55] which is also used to perform all the following simulations in this study. The granular assembly is isotopically compacted to a predefined stress state, using the so-called wall-servo mechanism, which is a way of adpaptively moving walls to compact the specimen to the a prescribed confining stress state [55, 56]. The default time step in PFC software is used in all the following numerical tests, and this default value is dependent on the current contact stiffnesses used, masses and sizes of all particles in the system [55]. Note an *initial coefficient of friction* is used to generate the granular specimens with different porosities [57-60]. By performing a sequence of numerical models with different initial friction coefficients (from 0 to 1), the porosity in the whole domain can be calculated from the eatablished models. The relations between the initial friction coefficient and porosity of the specimens are obtained as shown in Fig. 4. To prevent possible rearrangements of particles (irreversible plastic deformation) for the granular system subjected to a small strain condition, the initial

coefficient of friction is then replaced with a relatively larger coefficient of friction (e.g. 1.0), prior to performing loading and unloading tests. The model parameters adopted are listed in Table 1.

The axial deviatoric stress versus the axial strain is shown in Fig. 5, indicating that the specimen subjected to an axial strain of 5×10^{-4} is under an elastic state. This check is always recommended for a specific model due to two reasons: (1) the specimen before testing may not be in a sufficiently converged state (may interfering the initial stress-strain curves); (2) the model porosities affect the range of the elastic region. i.e, the elastic region for a loose model may stop at a relatively small axial strain while the counterpart for a dense model exists even if under a relatively large axial strain.

A loading rate of 5×10^{-5}m/s is applied to the loading walls (both upper and lower walls). The loading rate is chosen to make the model in a quasi-static state. To make a comprehensive comparison between our proposed formula and the numerical values, we perform a large number of tests with various porosities and stiffness ratios (K_s/K_n). In addition, the vertical components of the elastic stiffness matrix from the generalised kinematic solutions, the simplified kinematic solutions, a static solution documented in [26], and the numerical DEM solutions are compared. Figures 6 and 7 show the variations of the vertical component of the stiffness matrix (C_{2222} in the 2D or C_{3333} in the 3D model) with different porosities and stiffness ratios (K_s/K_n).

The results show that the differences between the generalised kinematic solution and the simplified kinematic solution are very small in DEM models with different porosity values and stiffness ratios, which indicates that our simplified kinematic solution is reliable.

Although significant differences can be found between the numerical results and analytical solutions (kinematic and static solutions), the derived kinematic solutions

are observed to predict the trend of elastic constants better than the static solutions in DEM specimens with varied K_s/K_n ratios.

From the perspective of continuum mechanics, the static hypothesis tends to yield a lower bound solution compared to the exact solution, while the kinematic solution derived from Voigt's hypothesis corresponds to an upper solution [61, 62]. It is natural to expect that the numerical DEM solution should be an intermediate value between the lower and upper bound solutions. However, Figs. 6 and 7 show that the analytical solutions (both kinematic and static solutions) always overpredict the elastic constants of granular matter. The mechanism behind these differences will be discussed in Section 3.2.

3.3 Polydisperse particle packing

A granular packing with varied sizes (polydisperse) is of more interests in engineering applications. Although the formulas (21)-(23) are derived based on the condition that the particles are equal-sized, they are extended here for polydisperse packings with the particle diameter $2r$ being replaced by the median diameter (d_{50}) of the polydisperse granular packing. To find out how much error may be introduced by such an extension, several tests are conducted with various uniformity coefficients (C_u) but a fixed d_{50}:

$$C_u=d_{60}/d_{40} \tag{28}$$

where d_{60} and d_{40} are the diameters below 60% and 40% of the total particles, respectively. The particle size distributions adopted for the simulations are shown in Table 2. The initial friction coefficient, normal and tangential particle stiffnesses are taken as 0.01, 1×10^8Pa and 5×10^7Pa, respectively.

The errors of using both the original kinematic solution and the simplified kinematic

solution are compared with the numerical solutions (see Fig.8). As Cu increases, the original kinematic solution gives a worse estimation but the simplified kinematic solution predicts the numerical solution better. The simplification that uses d50 to replace the distance between two arbitrary particles in Eqs. (21)-(23) may give rise to a relatively lower estimation. Such an underestimation compensates the error originally arising from the kinematic hypothesis. Therefore, although the formulas (21)-(23) are derived from the monodisperse packing, they can still provide relatively reliable estimations of macro material parameters for granular packings.

3.4 Mechanism responsible for differences between analytical and numerical solutions

External loads are transferred in granular materials in a way totally different from that in continuum media [63-65]. Figure 9 shows a two-dimensional granular experiment using binary photo-elastic discs. These discs in a box are subjected to pure shear deformation: the discs are squeezed vertically while being expanded with an equal horizontal velocity so that the total area remains constant.

The colours of the discs in experiments become brighter when subjected to greater contact forces. The figure shows that several column-like particle chains undergo significantly greater contact forces compared to most particles in the system. The load transfer mechanism in the granular medium exhibits significantly discontinuous and inhomogeneous features.

The analytical solutions are developed based on the homogenisation or averaged assumption which accounts for all the mechanical contacts equally. The nature of only a portion of strong contacts involved in transferring the external loads explains why considering weak contacts equally as strong contacts will make the derived equivalent stiffnesses overpredicting the actual value.

4 Refined estimations of linear contact stiffnesses with a numerical strategy

4.1 The closed-form formulation of particle-scale stiffnesses

In material science and physics, the macroscopic description of the deformation behaviour of granular materials is important. On the contrary, in DEM simulations for geo-materials, a more practical concern is how to estimate the values of stiffness parameters in contact models for particles, based on the macroscopic material properties.

From Eqs. (22) and (23), the particle-scale stiffnesses can be obtained as

$$\begin{cases} K_n = \dfrac{ES}{2N_c r^2 (1-2\nu)} \\ K_s = \dfrac{ES(1-7\nu)}{2N_c r^2 (1-\nu-2\nu^2)} \end{cases} \quad \text{(2D)} \tag{29}$$

$$\begin{cases} K_n = \dfrac{3EV}{4N_c r^2 (1-2\nu)} \\ K_s = \dfrac{3EV(1-4\nu)}{4N_c r^2 (1-\nu-2\nu^2)} \end{cases} \quad \text{(3D)} \tag{30}$$

Note that the values of N_c and V (or S) are not known *in prior* unless the model has been generated, but an estimation of S/N_c (2D) or V/N_c (3D) from empirical formulas is possible. Particularly, the median radius ($d_{50}/2$) can take the place of the particle radius r in Eqs. (29) and (30) to obtain approximations for K_n and K_s in granular materials with a varied particle size distribution, as is done in Section 3.1.3. This scheme will be further verified in Section 4.3.3.

4.2 The estimation of (S/N_c) or (V/N_c) based on randomly distributed specimens

The ratio of S/N_c (2D) or V/N_c (3D) governs the density of the granular packing and can be described by the coordination number $\bar{N}_c$ and the porosity ϕ. As two particles

can only form one contact, the coordination number $\bar{N}_c$ and the porosity ϕ are defined by:

$$\bar{N}_c = \frac{2N_c}{N_p} \tag{31}$$

$$\phi = \begin{cases} \frac{S_v}{S} & \text{(2D)} \\ \frac{V_v}{V} & \text{(3D)} \end{cases} \tag{32}$$

where N_p is the total number of particles, and S_v or V_v is the total area/volume of the voids. Assuming that the area/volume of a particle is S_p or V_p, then $V = V_V + V_P$ or $S = S_V + S_P$. For a monodisperse granular packing, the total particle area/volume can be determined by:

$$\begin{cases} S_p = N_p \pi r^2 & \text{(2D)} \\ V_P = N_p \frac{4}{3} \pi r^3 & \text{(3D)} \end{cases} \tag{33}$$

Combining Eqs. (31)-(33), the ratio of S/N_c (2D) or V/N_c (3D) is given by:

$$\begin{cases} \frac{S}{N_c} = \frac{2\pi r^2}{(1\text{-}\phi)\bar{N}_c} & \text{(2D)} \\ \frac{V}{N_c} = \frac{8\pi r^3}{3(1\text{-}\phi)\bar{N}_c} & \text{(3D)} \end{cases} \tag{34}$$

For a randomly distributed granular assembly, although the relationship between the porosity ϕ and the coordination number $\bar{N}_c$ is not unique, a proportional relationship has been proven to exist [33, 66]. As the porosity of a granular assembly is highly influenced by the initial friction coefficient, the relation between the packing related parameter $1/(1\text{-}\phi)\bar{N}_c$ and the numerical initial friction coefficient is investigated in the pre-stated benchmark models with a large range of porosity.

Figure 10 shows that a quadratic relation is found in both 2D and 3D cases. The

relevant fitted relation can provide a satisfactory estimation for the packing parameter $1/(1-\phi)\bar{N}_c$ in randomly distributed granular packings. The actual porosity in a granular packing may slightly vary with the changes in the particle size distribution, particle numbers involved in models, and confining stress conditions, and thus the empirical formulas in Fig. 10 is simply an estimation. If the estimation made by the provided empirical relations is found to be unsatisfactory during the following iterative computations, a remedial measure can be taken by choosing the actual value of S/N_c (2D) or V/N_c (3D) in the already generated model as a new approximation. Moreover, the approximation errors will be effectively reduced by the iterative scheme to be introduced in Section 4.3.

With the use of the empirical estimations for the packing related parameter $1/(1-\phi)\bar{N}_c$, the initial approximation values for the particle-scale parameters K_n and K_s can be given before generating the DEM model. These derived values will act as the initial guess for the iterative computational scheme proposed below to further improve the estimation for K_n and K_s.

4.3 **Using gradient descent to estimate particle-scale stiffnesses**

4.3.1 Error function and gradient descent scheme

The calibration process of particle-scale parameters for a granular assembly is equivalent to finding suitable parameter values to minimise the difference between the targeted macro-scopic behaviour and the actual behaviour. Thus the following *error or cost function* is constructed:

$$L(E^*,\nu^*) = \beta_1\left(\frac{E^*}{E}-1\right)^2 + \beta_2\left(\frac{\nu^*}{\nu}-1\right)^2 \tag{35}$$

where E^* and ν^* are the equivalent Young's modulus and Poisson's ratio of the granular assembly; E and ν are the targeted Young's modulus and Poisson's ratio; β_1

and β_2 are two positive weighting coefficients with $\beta_1 + \beta_2 = 1$. When only the targeted Young's modulus is required, β_1=1 and $\beta_2 = 0$. When both modulus and Poisson's ratio are of equal importance, β_1=β_2=0.5. As E^* and ν^* both are functions of K_n and K_s, the calibration process is now reduced to solve the minimisation problem (35), and thus many numerical methods can be used. In this work, the gradient descent scheme is adopted due to its simplicity.

To find the minimum of a function using gradient descent, independent variables are iteratively updated in the opposite direction of the gradient (or approximate gradient) of the function. The iterative procedure can be described as:

$$x_i := x_i - \eta_i \frac{\partial L}{\partial x_i} \tag{36}$$

where x_i is an independent parameter; the symbol ":= " means *assignment*; η_i is a learning rate to determine the size of the iterative step to be taken to reach a minimum; $\frac{\partial L}{\partial x_i}$ represents the derivative or gradient of the function along the x_i direction.

Due to highly non-linear and discontinuous features of the error function, three modifications are made to the above gradient descent algorithm to enhance the practicability and convergence.

The first measure is *scaling*. Both K_n and K_s are normalised by the initial values of K_n and K_s (denoted as $\bar{K}_n$ and $\bar{K}_s$, and given by Eqs. (29) and (30)), and the resulting normalised normal and tangential stiffnesses k_n and k_s are expressed as:

$$k_n = \frac{K_n}{\bar{K}_n},\ k_s = \frac{K_s}{\bar{K}_s} \tag{37}$$

Now the error function can be rewritten as:

$$L(E^*, \nu^*) = F(K_n, K_s) = f(k_n, k_s) \tag{38}$$

The second modification is that the gradient of the error function is approximated

by using the finite-difference method [67], i.e., the partial derivatives of the error function are given as:

$$\begin{cases} \dfrac{\partial L}{\partial k_n} \approx \dfrac{1}{\Delta k_n}\left[f(k_n, k_s) - f(k_n - \Delta k_n, k_s) \right] \\ \dfrac{\partial L}{\partial k_s} \approx \dfrac{1}{\Delta k_s}\left[f(k_n, k_s) - f(k_n, k_s - \Delta k_s) \right] \end{cases} \tag{39}$$

where Δk_n and Δk_s are (small) increments of the normalised particle stiffnesses k_n and k_s. At the first iteration, Δk_n and Δk_s are set to be $\Delta k_n = -\alpha K_n$ and $\Delta k_s = -\alpha K_s$ where the parameter α is typically taken around ~0.2. For other iterations, Δk_n and Δk_s are taken to be the step increments of k_n and k_s. This means that the gradient of the error function is approximated by its secant slope.

In the final modification, the increments in each iterative step are changed to

$$\begin{cases} \Delta k_n = -\eta_n L \dfrac{\partial L}{\partial k_n} \\ \Delta k_s = -\eta_s L \dfrac{\partial L}{\partial k_s} \end{cases} \tag{40}$$

where the learning rate η_i is chosen to be a constant and further multiplied by the error function. This modification to the step size is motivated by the fact that if the error function is sufficiently smooth, $\dfrac{\partial L}{\partial k_n}$ and $\dfrac{\partial L}{\partial k_s}$ will be equal to zero and $\Delta kn = \Delta ks = 0$ at the minimum value, but this smoothness assumption may not be valid in the current situation. Thus the presence of the error function effectively reduces the size of the learning step when the error function approaches to its minimum, leading to a more robust scheme with better convergence.

Then the particle stiffnesses in each iterative step are given by:

$$\begin{cases} k_n := k_n + \Delta k_n \\ k_s := k_s + \Delta k_s \end{cases} \tag{41}$$

When k_n and k_s are converged, the estimated values of K_n and K_s can be obtained by

the substitution of Eq. (37).

4.3.3 The implementation procedures

To develop the above-proposed methodology into a standard calibration procedure, we summarise the numerical steps involved in Fig.11. First, we take the experimentally determined Young's modulus and Poisson's ratio as the target values for the granular system concerned. By using the empirical relations of S/N_c or V/N_c, we can estimate reasonable initial values (K_n, K_s) for the particle-scale stiffnesses based on a desired porosity in the model according to Eq. (29) for 2D or Eq. (30) for 3D. A sequence of estimations to K_n and K_s can be obtained by the iterative procedure Eq. (41) until the error function $L(E^*,v^*)$ is smaller than a pre-defined tolerance. At each iterative step, standard DEM simulations such as biaxial or triaxial tests are performed to obtained both E^*,v^* for the given values of K_n and K_s.

4.4 Numerical tests of the proposed method

Four numerical cases (see Fig. 12), including a monodisperse random packing (case 1 and case 3), a polydisperse random packing (case 2) and a three-dimensional monodisperse packing with random distribution (case 4), are performed to show the robustness of the proposed method. The targeted Young's modulus and Poisson's ratio are 10GPa and 0.2, respectively, for all the test cases. Furthermore, the iterative process is terminated when the error function is less than 10^{-4}.

Case 1: Monodisperse random packing

A monodisperse granular packing with 1833 particles (the radius is 0.1m, the initial coefficient of friction is 0.1) is randomly generated in a square container and

isotropically consolidated to a uniform stress state of 1MPa. The parameters α_n, α_s, learning rates η_n and η_s are taken as 0.22, 0.22, 0.001 and 0.001, respectively. The predicated K_n and K_s and the errors during the iterative process are listed in Table 3.

Case 2: Polydisperse random packing

A random packing of 1655 particles with radii evenly distributed from 0.05m to 0.1m and the initial coefficient of friction 0.1 is generated in a square container and isotropically consolidated to a bi-axial stress level of 1MPa. The parameters α_n, α_s, learning rates η_n and η_s are taken as 0.2, 0.2, 0.001 and 0.001, respectively. The convergent histories of K_n and K_s and the errors are shown in Table 4.

Case 3: Estimating K_n and K_s with only the elastic modulus of a polydisperse packing

The elastic modulus and Poisson's ratio can be easily measured for solid, but are often difficult for granular assemblies, and also the obtained values may not be sufficiently accurate. When Poisson's ratio is not available or its value is not reliable, the proposed method can estimate K_n and K_s by setting β_1=1 and β_2=0 in the error function. A granular assembly with the particle radii evenly distributed from 0.05m to 0.1m is generated to show the capability of our proposed method to estimate K_n and K_s to only match Young's modulus. The parameters α_n, α_s, learning rates η_n and η_s are taken as 0.24, 0.24, 0.001 and 0.001, respectively. The convergent histories of K_n and K_s and the errors are shown in Table 5.

Case 4: Estimating K_n and K_s with the elastic modulus of 3D monodisperse packing

A three-dimensional monodisperse granular assembly is generated to show the iterative process of the proposed method. 4369 particles with a radius of 0.25m are

randomly distributed in the model. The 3D specimen is isotropically consolidated to a uniform stress state of 1MPa. The parameters α_n, α_s, learning rates η_n and η_s are taken as 0.1, -0.5, 0.01 and 0.01, respectively. The convergent histories of K_n and K_s and the errors are shown in Table 6.

The evolution histories of the error function during the iterative process for all the four cases are depicted in Fig. 13. Clearly, the error functions are not monotonically decreasing, due to nonlinear and discontinuous features of the relationship between the meso-scopic contact stiffnesses and the macro-scopic material properties. However, the error function in all the cases exhibits a significant decrease from a relatively large initial value to a value less than 10^{-4}. The tests show that the proposed framework for the estimation of linear contact stiffnesses is practicable and effective for both monodisperse and polydisperse packings. Note, however, that the choice of the parameters α_n, α_s, η_n and η_s will affect the convergence of the iterative procedure.

5 Concluding Remarks

A hybrid analytical-computational method has been proposed to calibrate the linear contact stiffnesses K_n and K_s for DEM simulations. Based on the derived semi-analytical and semi-empirical formula, a reasonable initial estimation to K_n and K_s can be obtained. By taking their values as the initial guess, K_n and K_s can be iteratively refined by using the gradient descent method to minimise the error function which measures the difference between the achieved equivalent macroscopic parameters (Young's modulus and Poisson's ratio) and the targeted values. The proposed framework has been validated and confirmed to be applicable to randomly generated monodisperse and polydisperse packings.

The effectiveness of this proposed hybrid calibration method is attributed to both

factors: one is that the derived analytical formulas provide an initial guess close to true parameters. The other one is that the gradient-based iterative algorithm offers chances to optimise the parameters continuously. Both factors are indispensable for a successful calibration. Without a relatively accurate initial guess, the optimisation algorithm may suffer from unpredictable local optimums and possible divergence. On the other hand, without the use of an optimisation algorithm, the derived continuum-based analytical solution may significantly under- or over-predict the actual parameters, due to its inability to account for wide range changes in porosity, particle-scale K_s/K_n ratio, the particle number and randomness in DEM models.

This proposed hybrid framework is generic and flexible in which any effective optimisation algorithms can be adopted to improve the prediction of the model parameters. The methodology can also be extended to other parameter calibration problems in DEM.

References

[1] M. Marigo, E.H. Stitt, Discrete element method (DEM) for industrial applications: comments on calibration and validation for the modelling of cylindrical pellets, Kona Powder Part J, 32 (2015) 236-252.

[2] C. Coetzee, Calibration of the discrete element method and the effect of particle shape, Powder Technology, 297 (2016) 50-70.

[3] C.J. Coetzee, Review: Calibration of the discrete element method, Powder Technology, 310 (2017) 104-142.

[4] J. Quist, M. Evertsson, Framework for DEM model calibration and validation, Proceedings of the 14th European Symposium on Comminution and Classification, Gothenburg, Sweden, 2015, pp. 103-108.

[5] C. O'Sullivan, Particulate discrete element modelling: a geomechanics perspective, CRC Press2014.

[6] T. Roessler, C. Richter, A. Katterfeld, F. Will, Development of a standard calibration procedure for the DEM parameters of cohesionless bulk materials–part I: Solving the problem of ambiguous parameter combinations, Powder Technology, 343 (2019) 803-812.

[7] M. Dosta, U. Bröckel, L. Gilson, S. Kozhar, G.K. Auernhammer, S. Heinrich, Application of micro computed tomography for adjustment of model parameters for discrete element method, Chemical Engineering Research and Design, 135 (2018) 121-128.

[8] M. Ismail, Z. Mohamed, M. Razali, Contact stiffness parameters of soil particles model for discrete element modeling using static packing pressure test, AIP Conference Proceedings, AIP Publishing, 2018, pp. 020014.
[9] T. Roessler, A. Katterfeld, DEM parameter calibration of cohesive bulk materials using a simple angle of repose test, Particuology, 45 (2019) 105-115.
[10] S. Wang, T. Qu, Y. Fang, J. Fu, J. Yang, Stress Responses Associated with Earth Pressure Balance Shield Tunneling in Dry Granular Ground Using the Discrete-Element Method, International Journal of Geomechanics, 19 (2019) 04019060.
[11] T. Qu, S. Wang, J. Fu, Q. Hu, X. Zhang, Numerical Examination of EPB Shield Tunneling–Induced Responses at Various Discharge Ratios, J Perform Constr Fac, 33 (2019) 04019035.
[12] T. Qu, S. Wang, J. Fu, Q. Hu, J. Yang, Numerical Investigation on Muck Pressures During EPB Shield Tunneling with Varying Discharge Ratio Based on Coupled PFC3D/FLAC3D Method, Springer International Publishing, Cham, 2019, pp. 204-213.
[13] T. Qu, Y. Feng, Y. Wang, M. Wang, Discrete element modelling of flexible membrane boundaries for triaxial tests, Computers and Geotechnics, 115 (2019) 103154.
[14] J. Yoon, Application of experimental design and optimization to PFC model calibration in uniaxial compression simulation, International Journal of Rock Mechanics and Mining Sciences, 44 (2007) 871-889.
[15] L. Benvenuti, C. Kloss, S. Pirker, Identification of DEM simulation parameters by Artificial Neural Networks and bulk experiments, Powder technology, 291 (2016) 456-465.
[16] H. Zhou, Z. Hu, J. Chen, X. Lv, N. Xie, Calibration of DEM models for irregular particles based on experimental design method and bulk experiments, Powder Technology, 332 (2018) 210-223.
[17] M. Rackl, K.J. Hanley, A methodical calibration procedure for discrete element models, Powder technology, 307 (2017) 73-83.
[18] A. Boikov, R. Savelev, V. Payor, DEM Calibration Approach: Random Forest, Journal of Physics: Conference Series, IOP Publishing, 2018, pp. 012009.
[19] J. Pachón-Morales, H. Do, J. Colin, F. Puel, P. Perré, D. Schott, DEM modelling for flow of cohesive lignocellulosic biomass powders: Model calibration using bulk tests, Adv Powder Technol, 30 (2019) 732-750.
[20] H.Q. Do, A.M. Aragón, D.L. Schott, A calibration framework for discrete element model parameters using genetic algorithms, Adv Powder Technol, 29 (2018) 1393-1403.
[21] H. Cheng, T. Shuku, K. Thoeni, H. Yamamoto, Probabilistic calibration of discrete element simulations using the sequential quasi-Monte Carlo filter, Granular matter, 20 (2018) 1-19.
[22] H. Cheng, T. Shuku, K. Thoeni, P. Tempone, S. Luding, V. Magnanimo, An iterative Bayesian filtering framework for fast and automated calibration of DEM models, Computer Methods in Applied Mechanics and Engineering, 350 (2019) 268-294.
[23] X. Li, H. Yu, X. Li, Macro–micro relations in granular mechanics, International Journal of Solids and Structures, 46 (2009) 4331-4341.
[24] P. Digby, The effective elastic moduli of porous granular rocks, Journal of Applied Mechanics, 48 (1981) 803-808.
[25] K. Walton, The effective elastic moduli of a random packing of spheres, Journal of the Mechanics and Physics of Solids, 35 (1987) 213-226.

[26] C.S. Chang, S.J. Chao, Y. Chang, Estimates of elastic moduli for granular material with anisotropic random packing structure, International journal of solids and structures, 32 (1995) 1989-2008.
[27] C.-L. Liao, T.-P. Chang, D.-H. Young, C.S. Chang, Stress-strain relationship for granular materials based on the hypothesis of best fit, International Journal of Solids and Structures, 34 (1997) 4087-4100.
[28] C.S. Chang, M. Lun, Elastic material constants for isotropic granular solids with particle rotation, International journal of solids and structures, 29 (1992) 1001-1018.
[29] N.P. Kruyt, L. Rothenburg, Statistical theories for the elastic moduli of two-dimensional assemblies of granular materials, International journal of engineering science, 36 (1998) 1127-1142.
[30] P. Chou, J. Carleone, C. Hsu, Elastic constants of layered media, Journal of composite materials, 6 (1972) 80-93.
[31] C.S. Chang, C.L. Liao, Estimates of elastic modulus for media of randomly packed granules, Applied Mechanics Reviews, 47 (1994) S197-S206.
[32] S. Yimsiri, K. Soga, Micromechanics-based stress strain behaviour of soils at small strains, Geotechnique, 50 (2000) 559-671.
[33] C.L. Liao, T.C. Chan, A.S. Suiker, C.S. Chang, Pressure‐dependent elastic moduli of granular assemblies, International Journal for Numerical and Analytical Methods in Geomechanics, 24 (2000) 265-279.
[34] I. Goldhirsch, C. Goldenberg, On the microscopic foundations of elasticity, The European Physical Journal E, 9 (2002) 245-251.
[35] A. Tanguy, J. Wittmer, F. Leonforte, J.-L. Barrat, Continuum limit of amorphous elastic bodies: A finite-size study of low-frequency harmonic vibrations, Physical Review B, 66 (2002) 174205.
[36] F. Radjai, S. Roux, Turbulentlike fluctuations in quasistatic flow of granular media, Physical review letters, 89 (2002) 064302.
[37] C. Goldenberg, A. Tanguy, J.-L. Barrat, Particle displacements in the elastic deformation of amorphous materials: Local fluctuations vs. non-affine field, EPL (Europhysics Letters), 80 (2007) 16003.
[38] F. Leonforte, A. Tanguy, J. Wittmer, J.-L. Barrat, Inhomogeneous elastic response of silica glass, Physical review letters, 97 (2006) 055501.
[39] B. Glasser, I. Goldhirsch, Scale dependence, correlations, and fluctuations of stresses in rapid granular flows, Physics of Fluids, 13 (2001) 407-420.
[40] A. Hershey, The elasticity of an isotropic aggregate of anisotropic cubic crystals, Journal of Applied mechanics-transactions of the ASME, 21 (1954) 236-240.
[41] J. Fleischmann, W. Drugan, M. Plesha, Direct micromechanics derivation and DEM confirmation of the elastic moduli of isotropic particulate materials: Part I No particle rotation, Journal of the Mechanics and Physics of Solids, 61 (2013) 1569-1584.
[42] M. Satake, A discrete-mechanical approach to granular materials, International journal of engineering science, 30 (1992) 1525-1533.
[43] K. Bagi, Stress and strain in granular assemblies, Mechanics of materials, 22 (1996) 165-177.
[44] X. Li, X.-S. Li, Micro-macro quantification of the internal structure of granular materials, Journal of engineering mechanics, 135 (2009) 641-656.
[45] C. Goldenberg, I. Goldhirsch, Force chains, microelasticity, and macroelasticity, Physical review letters, 89 (2002) 084302.
[46] C. Goldenberg, I. Goldhirsch, Friction enhances elasticity in granular solids,

Nature, 435 (2005) 188-191.
[47] S. Ouaguenouni, J.-N. Roux, Force distribution in frictionless granular packings at rigidity threshold, EPL (Europhysics Letters), 39 (1997) 117-122.
[48] Q. Sun, F. Jin, J. Liu, G. Zhang, Understanding force chains in dense granular materials, International Journal of Modern Physics B, 24 (2010) 5743-5759.
[49] H. Lankarani, P. Nikravesh, A contact force model with hysteresis damping for impact analysis of multibody systems, Journal of mechanical design, 112 (1990) 369-376.
[50] D. Griffiths, G.G. Mustoe, Modelling of elastic continua using a grillage of structural elements based on discrete element concepts, International Journal for Numerical Methods in Engineering, 50 (2001) 1759-1775.
[51] C. Song, P. Wang, H.A. Makse, A phase diagram for jammed matter, Nature, 453 (2008) 629-632.
[52] S. Luding, Micro–macro transition for anisotropic, frictional granular packings, International Journal of Solids and Structures, 41 (2004) 5821-5836.
[53] Q. Zhu, J.-F. Shao, M. Mainguy, A micromechanics-based elastoplastic damage model for granular materials at low confining pressure, International Journal of Plasticity, 26 (2010) 586-602.
[54] R. Bathurst, L. Rothenburg, Micromechanical aspects of isotropic granular assemblies with linear contact interactions, Journal of applied mechanics, 55 (1988) 17-23.
[55] Itasca, PFC3D—Particle Flow Code in 3 Dimensions, Version 5 Minneapolis, USA, 2014
[56] T. Qu, S. Wang, Q. Hu, Coupled Discrete Element-Finite Difference Method for Analysing Effects of Cohesionless Soil Conditioning on Tunneling Behaviour of EPB Shield, KSCE Journal of Civil Engineering, 23 (2019) 4537-4551.
[57] A. Soroush, B. Ferdowsi, Three dimensional discrete element modeling of granular media under cyclic constant volume loading: a micromechanical perspective, Powder technology, 212 (2011) 1-16.
[58] W. Yan, Fabric evolution in a numerical direct shear test, Computers and Geotechnics, 36 (2009) 597-603.
[59] X. Gu, M. Huang, J. Qian, DEM investigation on the evolution of microstructure in granular soils under shearing, Granular Matter, 16 (2014) 91-106.
[60] M. Hazeghian, A. Soroush, DEM simulation of reverse faulting through sands with the aid of GPU computing, Computers and Geotechnics, 66 (2015) 253-263.
[61] E.J. Barbero, Finite element analysis of composite materials, CRC press2007.
[62] N.P. Kruyt, L. Rothenburg, Micromechanical bounds for the effective elastic moduli of granular materials, International Journal of Solids and Structures, 39 (2002) 311-324.
[63] S. Luding, Granular media: Information propagation, Nature, 435 (2005) 159-160.
[64] J.F. Peters, M. Muthuswamy, J. Wibowo, A. Tordesillas, Characterization of force chains in granular material, Phys Rev E Stat Nonlin Soft Matter Phys, 72 (2005) 041307.
[65] J. Zhang, T. Majmudar, M. Sperl, R. Behringer, Jamming for a 2D granular material, Soft Matter, 6 (2010) 2982-2991.
[66] P.-Y. Hicher, C.S. Chang, Anisotropic nonlinear elastic model for particulate materials, Journal of Geotechnical and Geoenvironmental Engineering, 132 (2006) 1052-1061.
[67] Y. Feng, T. Zhao, J. Kato, W. Zhou, Towards stochastic discrete element

modelling of spherical particles with surface roughness: A normal interaction law, Computer Methods in Applied Mechanics and Engineering, 315 (2017) 247-272.

Tables

Table 1. Model parameters used

Parameters	2D model	3D model
Particle radius (m)	0.1	0.5
Initial model size (m)	8×8	20×20×20
Number of Particles	1833	7639
Normal stiffness (N/m)	10^8	10^8
Tangential stiffness (N/m)	$0.1\sim1\times10^8$	$0.1\sim1\times10^8$
Local damping	0.7	0.7

Table 2. Particle size distributions used in the simulations

Specimen	Particle size (m)	d_{50} (m)	C_u
1	0.18	0.18	1.00
2	0.16-0.2	0.18	1.12
3	0.14-0.22	0.18	1.27
4	0.12-0.24	0.18	1.45
5	0.10-0.26	0.18	1.69
6	0.08-0.28	0.18	2.00
7	0.06-0.30	0.18	2.43
8	0.04-0.32	0.18	3.06

Table 3. Estimation process of K_n and K_s in a monodisperse granular assembly

Iteration	K_n (N/m)	K_S (N/m)	Young's modulus (Pa)	Poisson's ratio	Modulus error	Poisson's ratio error
0	13352500	4450833	13479256	0.177	0.348	-0.114
1	10414950	3471650	9990477	0.236	-0.001	0.178
2	10414934	3471640	10494977	0.204	0.049	0.021
3	10182886	3431141	9976366	0.222	-0.002	0.112
4	10182882	3431143	10002330	0.217	0.000	0.087
5	9546649	3695261	9667307	0.209	-0.033	0.047
6	9546651	3695261	9751230	0.197	-0.025	-0.015
7	9588986	3662764	10016067	0.193	0.002	-0.037
8	9588985	3662765	9805469	0.200	-0.019	0.002
9	9605966	3687070	10005307	0.201	0.001	0.007

Table 4. Estimation process of K_n and K_s in a polydisperse granular assembly

Iteration	K_n (N/m)	K_S (N/m)	Young's modulus (Pa)	Poisson's ratio	Modulus error	Poisson's ratio error
0	13352500	4450833	12250834	0.200	0.225	-0.002
1	10682000	3560667	10032187	0.194	0.003	-0.028
2	10681999	3560666	10021518	0.209	0.002	0.043
3	10629690	3504728	9840505	0.211	-0.016	0.054
4	10629689	3504729	9740761	0.212	-0.026	0.062
5	10575279	3542058	9781819	0.216	-0.022	0.078
6	10575271	3542053	9821254	0.206	-0.018	0.029
7	10533175	3546570	9995560	0.198	0.000	-0.012

Table 5. Estimation process of K_n and K_s matching only the elastic modulus for a 2D monodisperse packing

Iteration	K_n (N/m)	K_s (N/m)	Young's modulus (Pa)	Modulus error
0	13352500	4450833	13479256	0.348
1	10147900	3382633	10167165	0.017
2	10147898	3382632	10135995	0.014
3	10149351	3383795	9905912	-0.009

Table 6. Estimation process of K_n and K_s matching only the elastic modulus for a 3D monodisperse packing

Iteration	K_n (N/m)	K_s (N/m)	Young's modulus (Pa)	Modulus error
0	8342918	1390486	10251664	0.025
1	7508626	2085730	11346501	0.135
2	7508123	2085075	11337610	0.134
3	6203517	2069598	10410624	0.041
4	6194155	2059840	10405686	0.041
5	6087605	2056510	9992706	-0.001

Figures

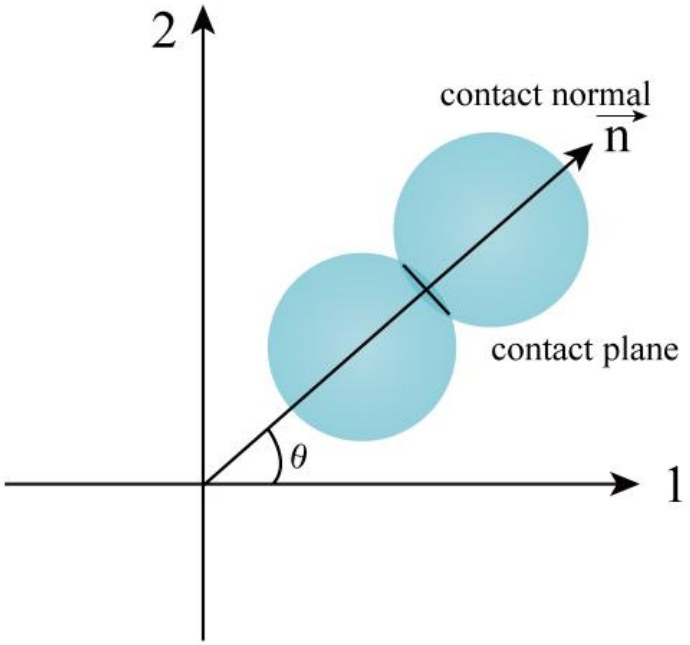

(a) 2D model

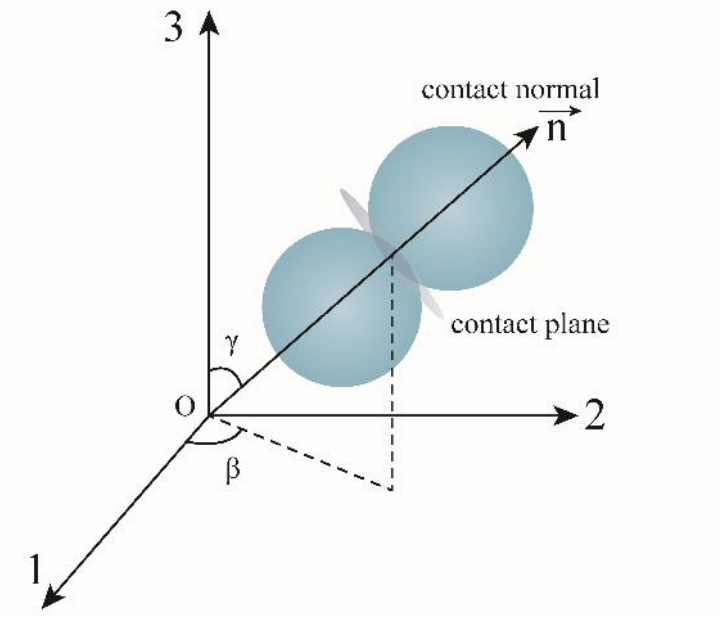

(b) 3D model

Fig. 1 Polar coordinate (2D) and spherical coordinate (3D) for directional distribution of inter-particle contacts

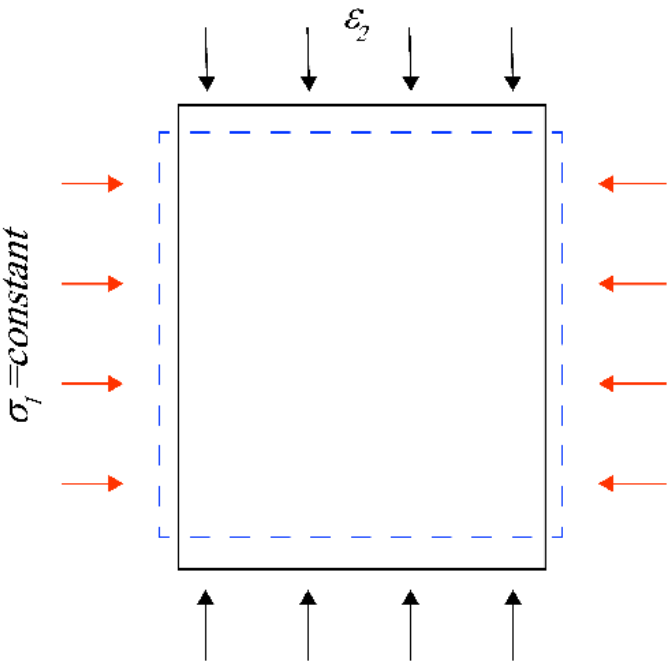

(a) Constant confining stress

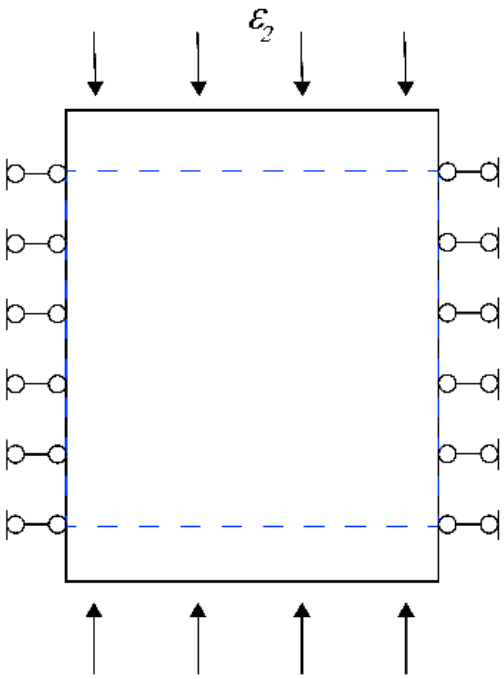

(b) Fixed lateral boundary

Fig.2 Schematic of biaxial testing case

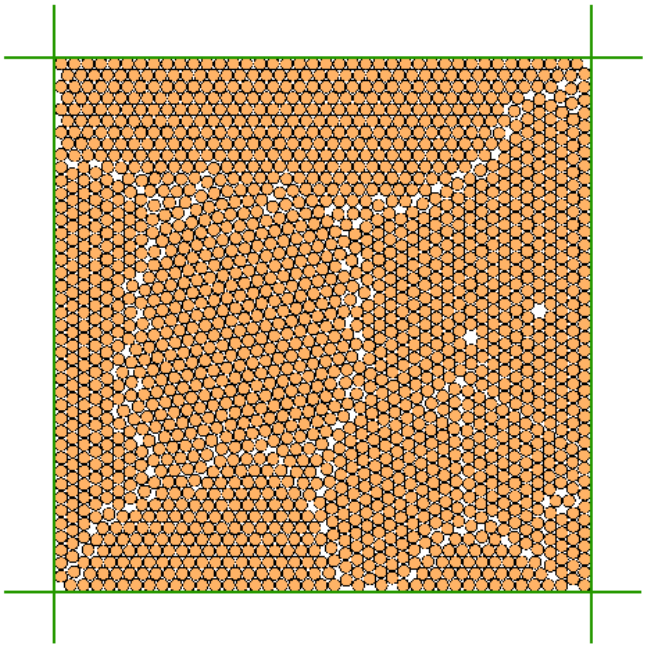

(a) 2D model

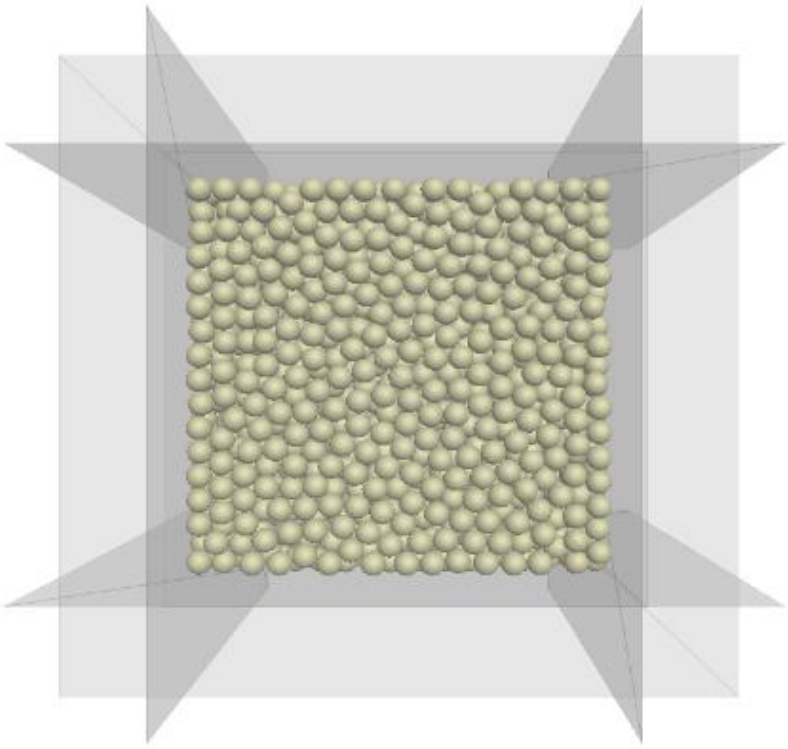

(b) 3D model

Fig.3 Benchmark models

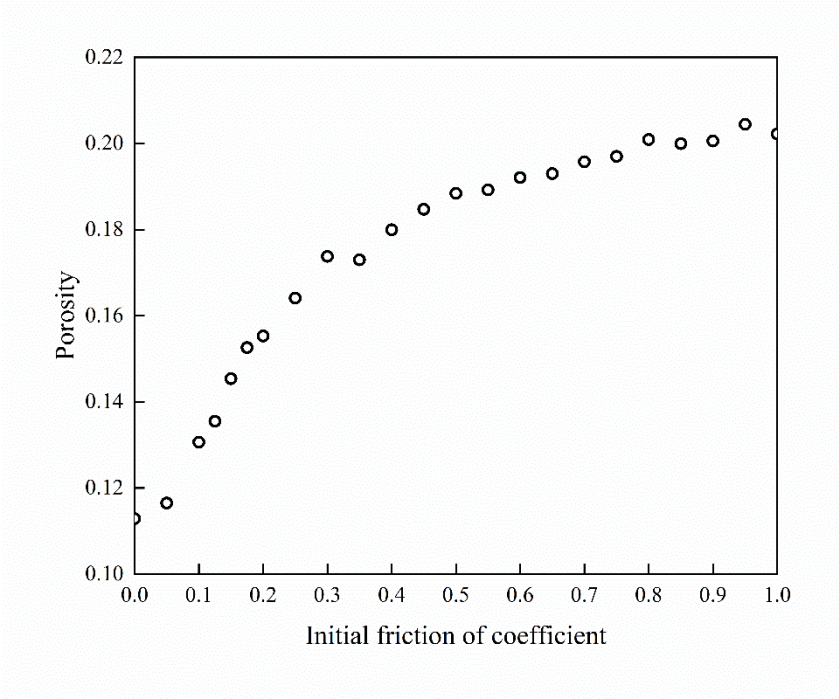

(a) 2D model

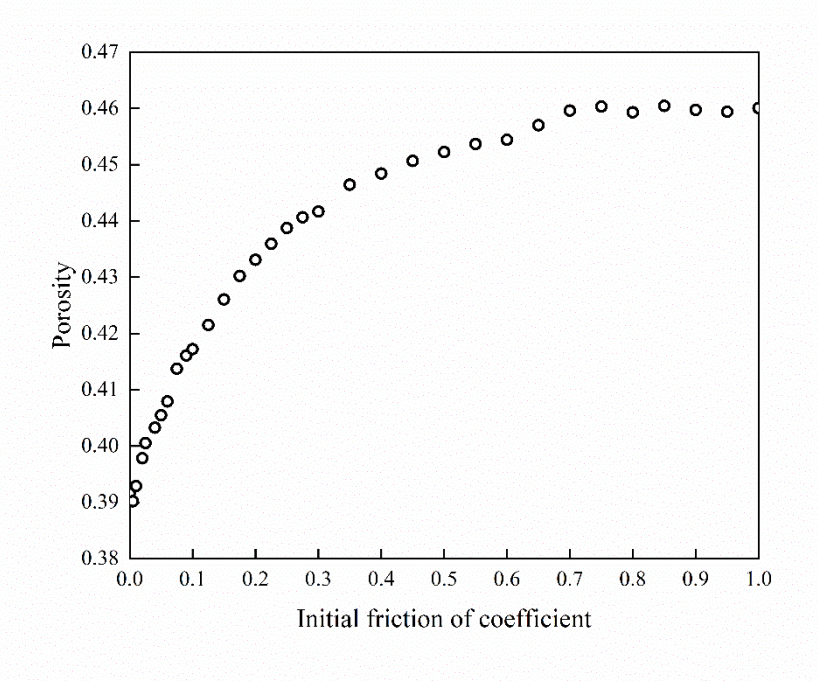

(b) 3D model

Fig. 4 The relations between initial coefficient of friction and porosity in specimens

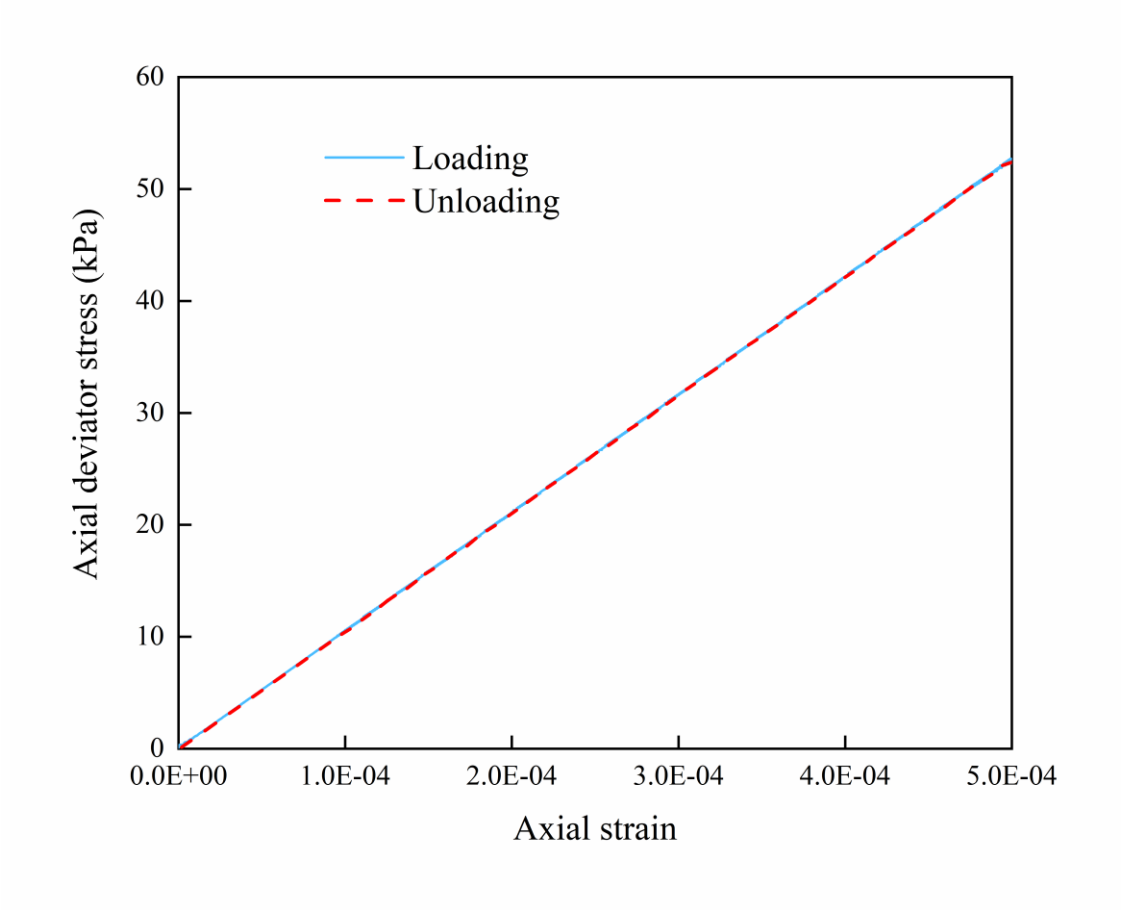

Fig.5 Axial deviatoric stress vs axial strain for elastic load/unload test (dense sample)

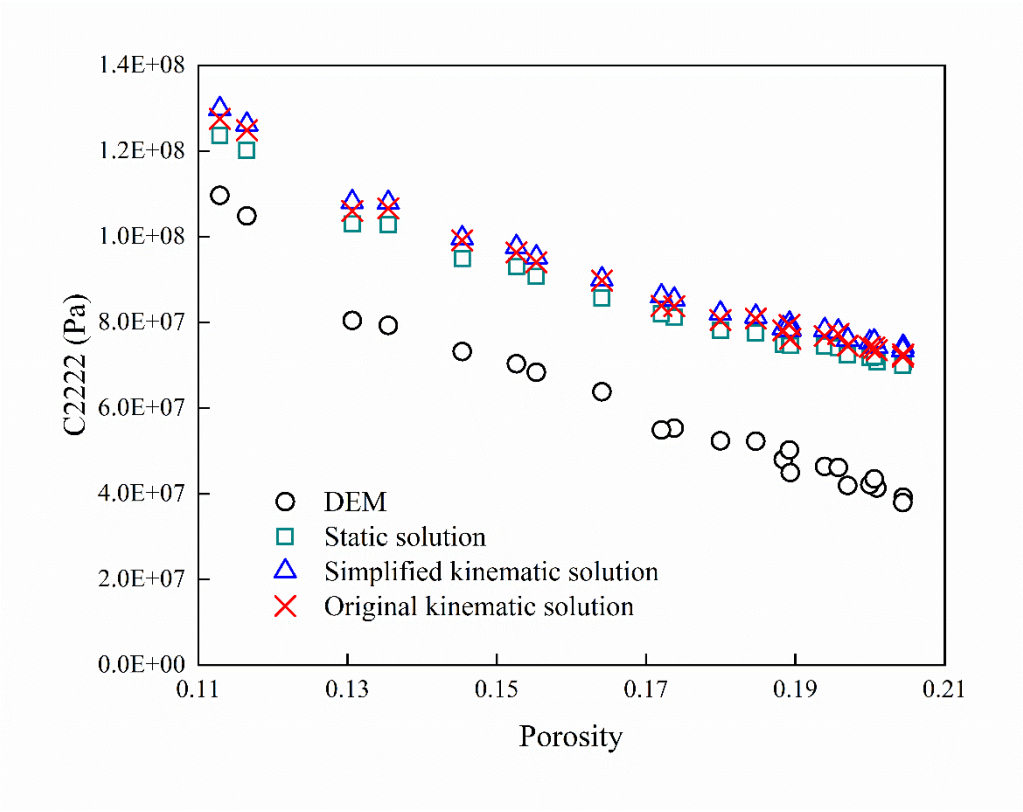

(a) 2D model

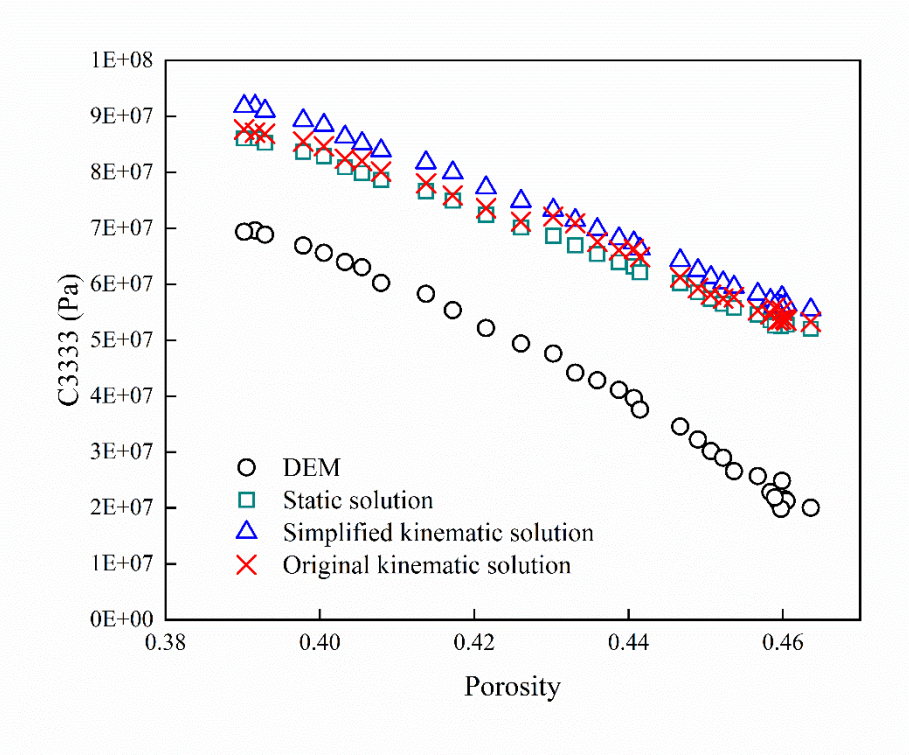

(b) 3D model

Fig. 6 Vertical component of equivalent stiffness tensor in DEM model with varied porosity

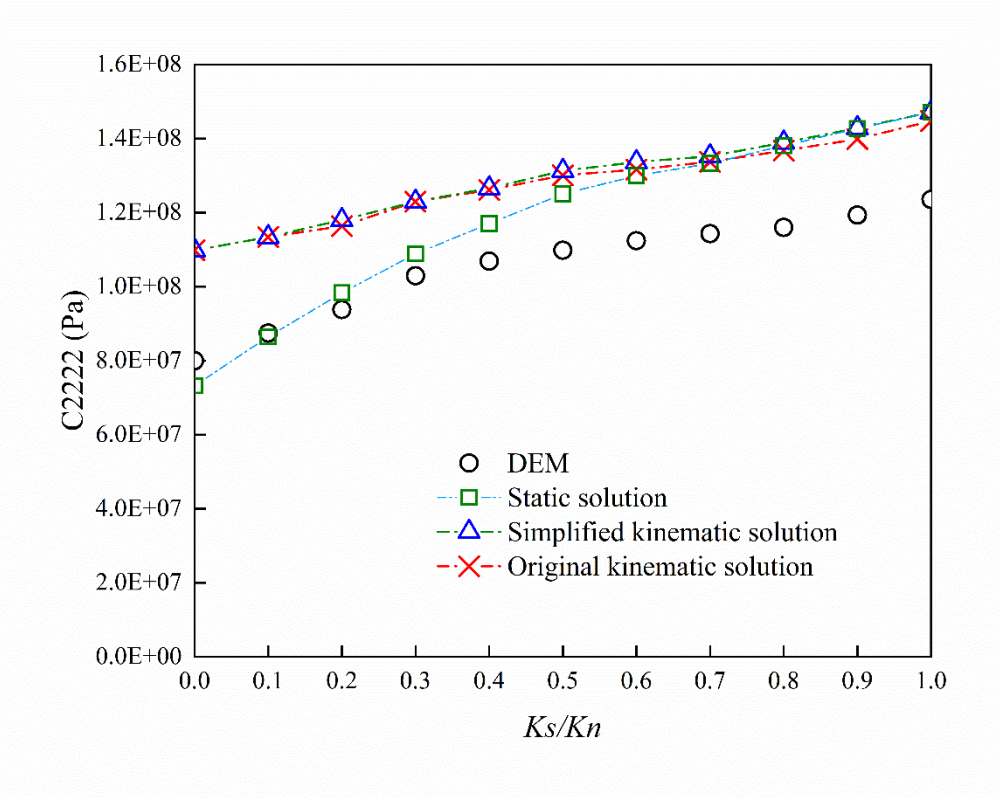

(a) 2D model

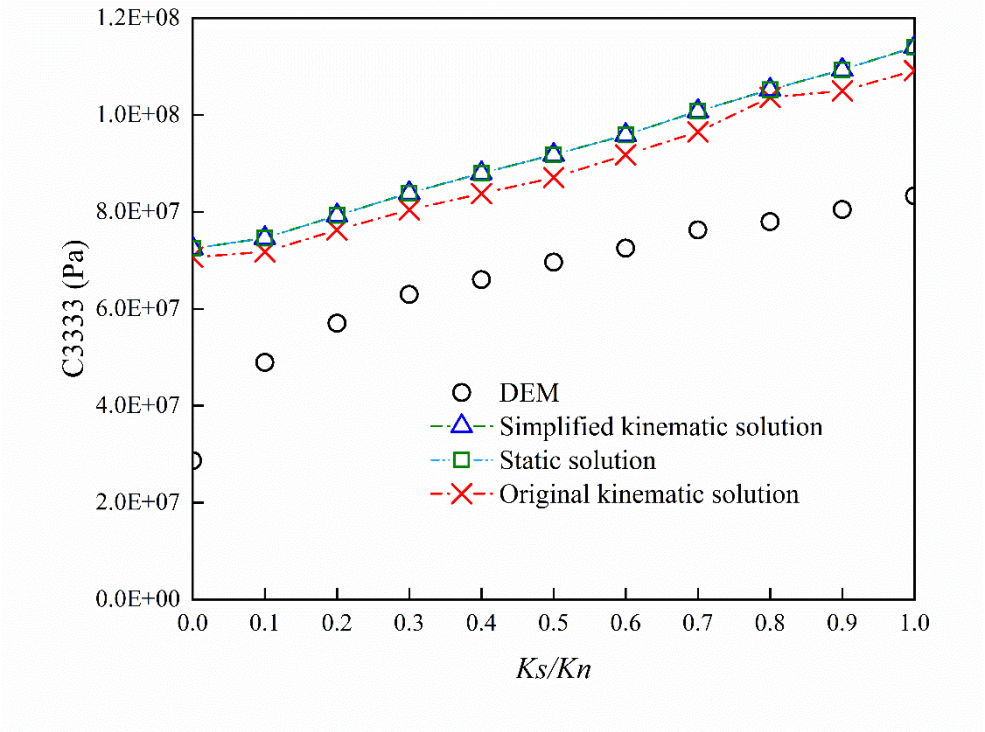

(b) 3D model

Fig. 7 The vertical component of equivalent stiffness tensor in DEM models with varied K_s/K_n ratio

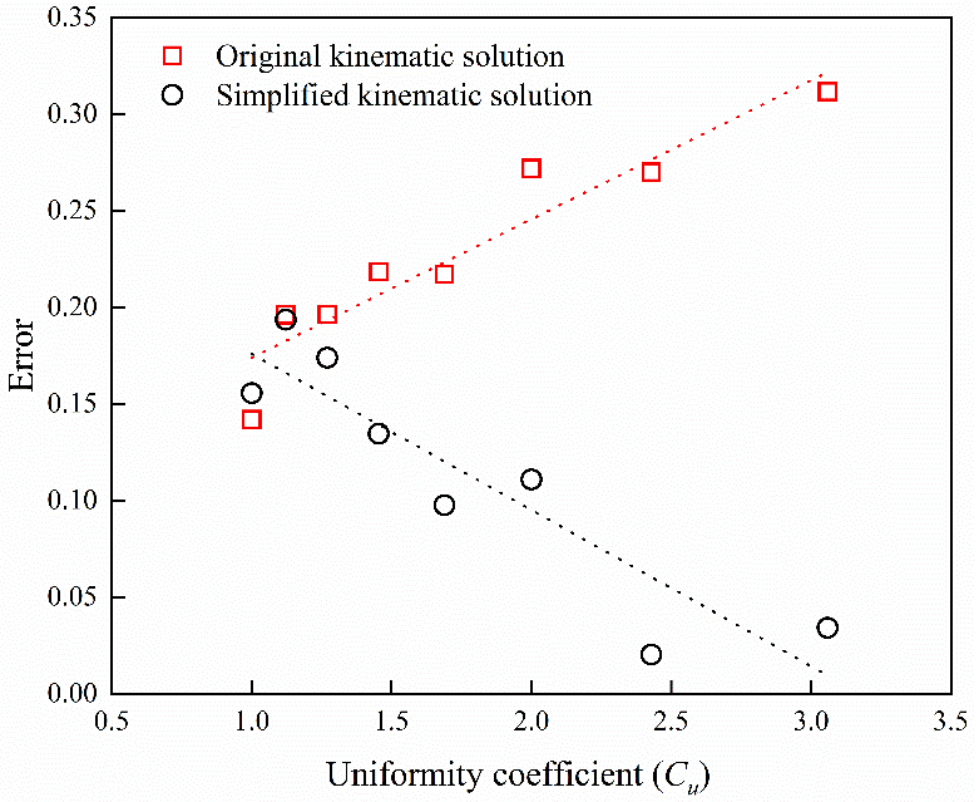

Fig. 8 The errors between the analytical solutions and the numerical solutions in the polydisperse packing

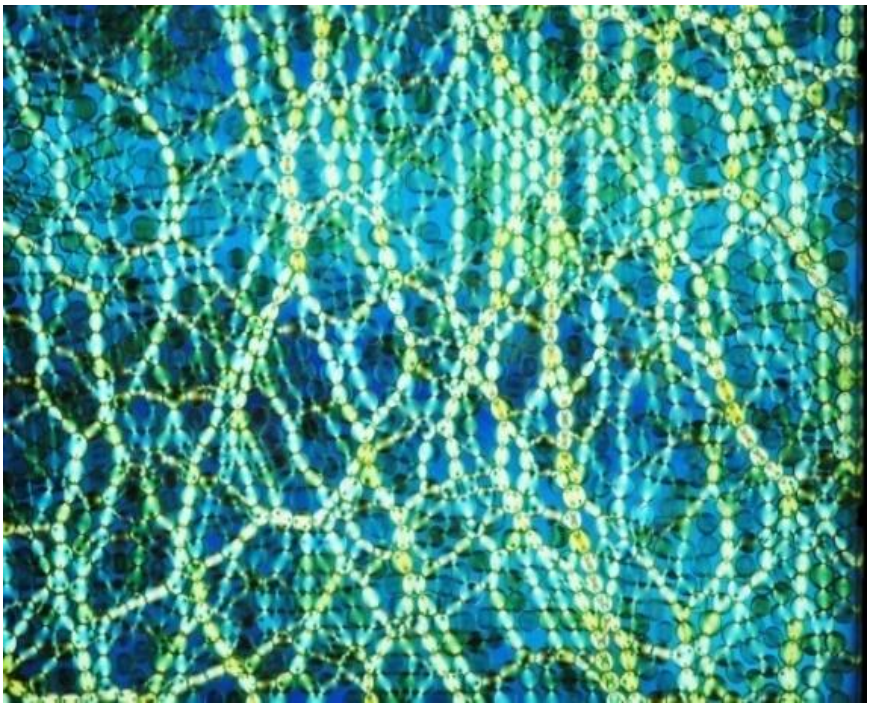

Fig.9 Load transfer in a granular solid subjected to pure shear deformation (photoelastic images)

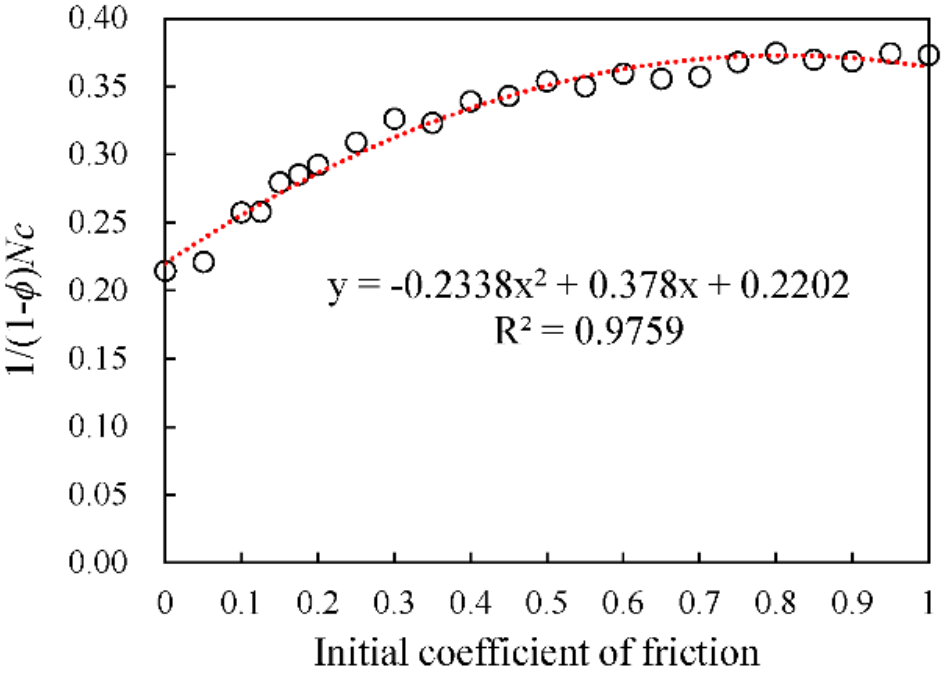

(a) 2D model

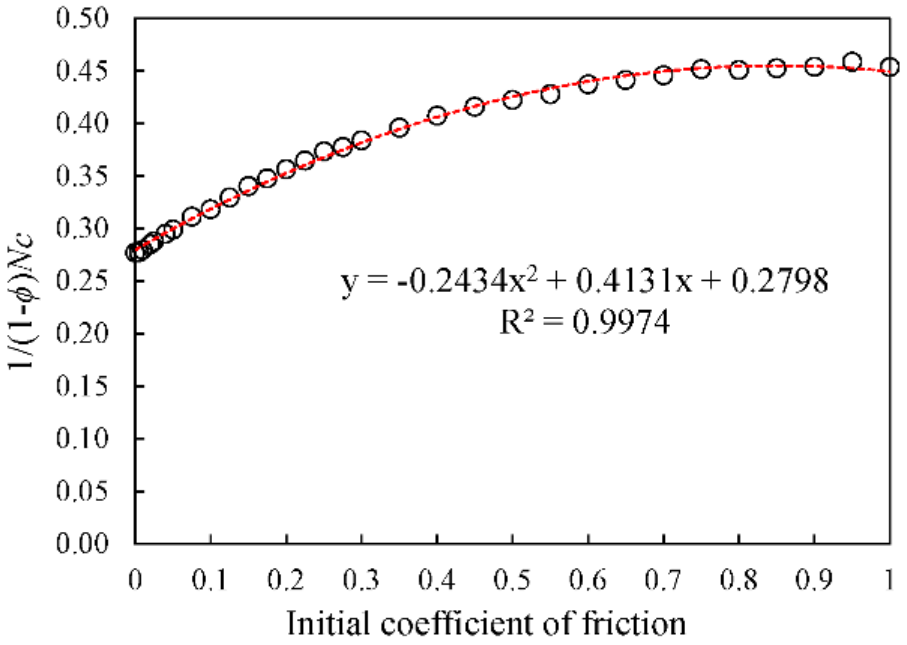

(b) 3D model

Fig. 10 The changes in packing parameter $1/(1-\phi)\bar{N}_c$ with varied porosity

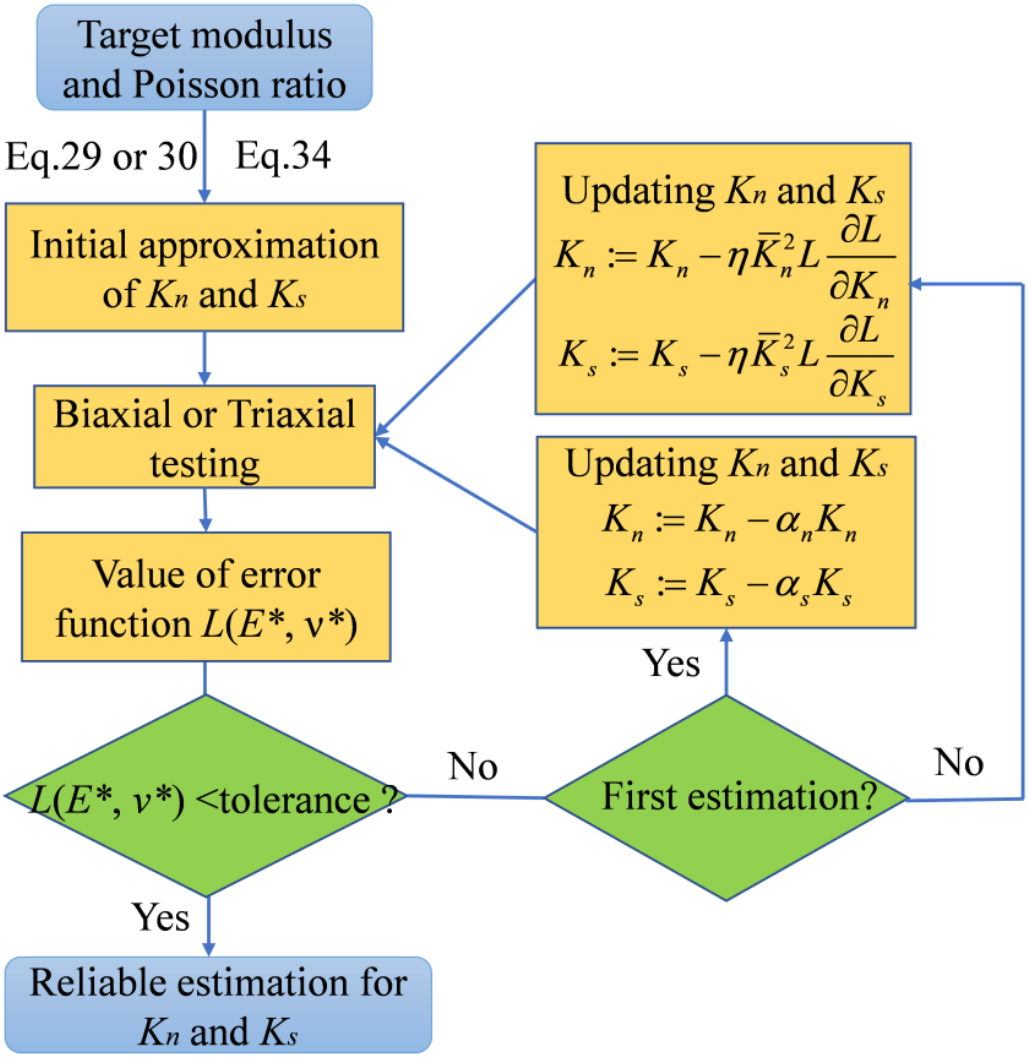

Fig. 11 Flow chart for iteratively determining K_n and K_s

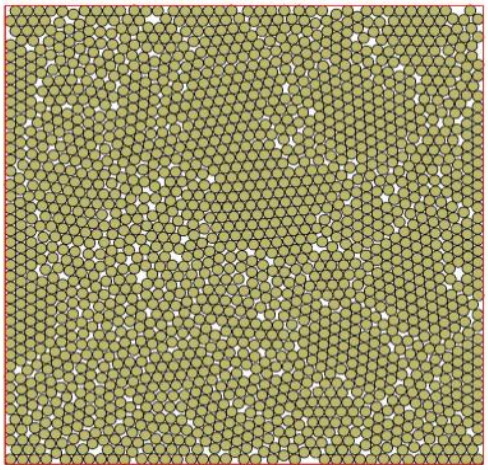

(a) case 1 and case 3

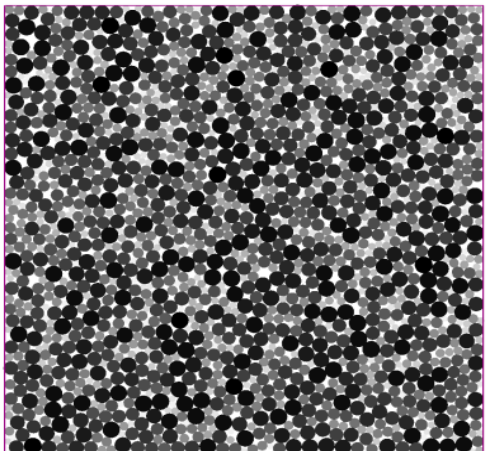

(b) case 2

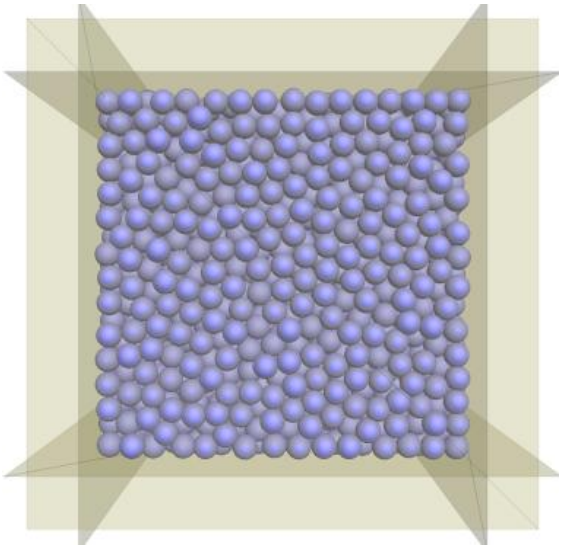

(c) case 4

Fig. 12 Granular packings used for tests: (a) random monodisperse packing; (b) random polydisperse packing; and (c) 3D random monodisperse packing

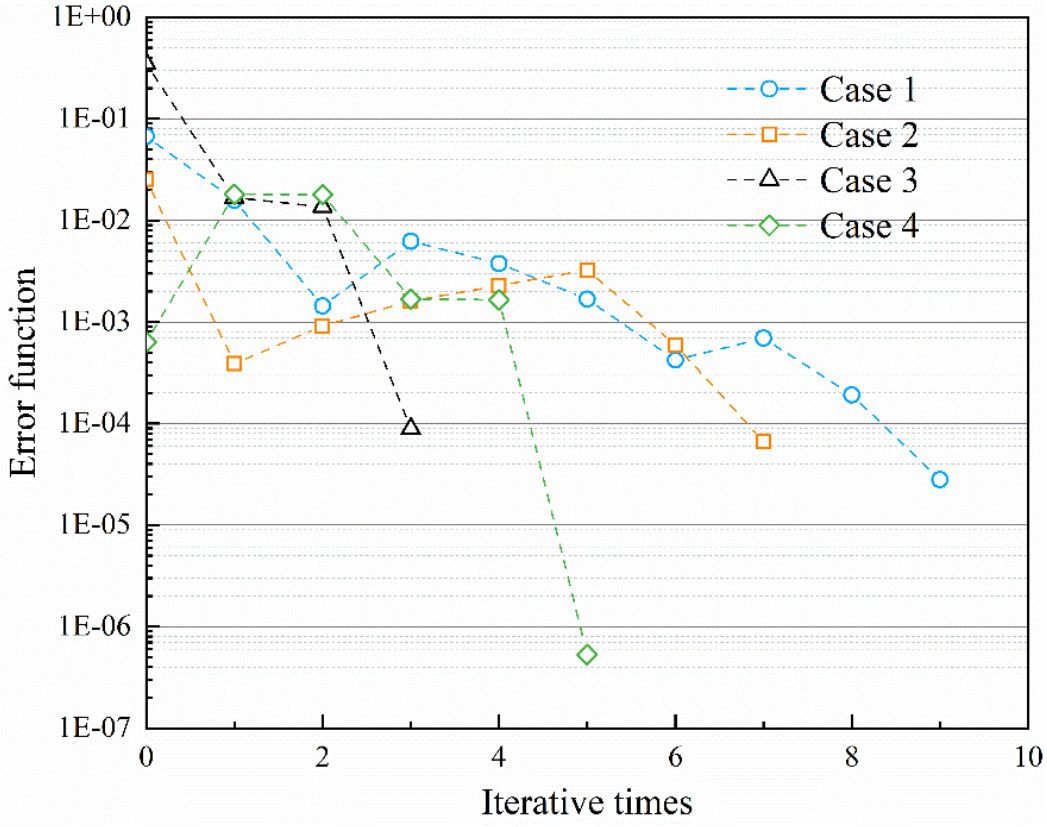

Fig. 13 The iterative processes for illustrated cases